이학석사학위논문

Effect of boron content on atomic structure of boron-bearing multicomponent oxide glasses: A view from the solid-state NMR

붕소를 함유한 용융체의 원자 환경 규명을 통한

마그마의 이동 물성의 미시적 근원: 고상 핵자기 공명 분광분석

2017 년 2 월

서울대학교 대학원

자연과학대학 지구환경과학부

이 아 침

Abstract

Effect of boron content on atomic structure of boron-bearing multicomponent oxide glasses: A view from the solid-state NMR

Lee, A Chim

School of Earth and Environmental Sciences

The Graduate School

Seoul National University

Understanding the effect of boron content on atomic structures of boron-bearing multicomponent silicate melts is essential to reveal the atomistic origins of diverse geochemical processes involving silica-rich magmas, such as explosive volcanic eruption and the reaction of magma in contact with aqueous solutions. It is also considered crucial in environmental science because a nuclear waste glasses contain B_2O_3. Despite the importance, the detailed atomic structure of boron-bearing multicomponent silicate glasses remains unsolved. We report experimental results on the effect of boron content on the atomic structures of sodium borate glasses and boron-bearing multicomponent silicate melts [nepheline ($NaAlSiO_4$)- malinkoite ($NaBSiO_4$) and albite ($NaAlSi_3O_8$)- reedmergnerite ($NaBSi_3O_8$) pseudo-binary glasses] using the high-resolution solid-state NMR (^{11}B, ^{27}Al, and ^{17}O). The ^{11}B NMR spectra of Na_2O-B_2O_3 glasses show that four-coordinated boron ($^{[4]}B$) increases at the expense of ring (three-coordinated boron, $^{[3]}B$) not of non-ring ($^{[3]}B$) with increasing sodium content based on the new interpretation from the results of quantum chemical calculations that ^{11}B NMR chemical shift of non-ring ($^{[3]}B$) increases with increasing sodium content. The two topological species of $^{[4]}B$ are firstly observed in ^{11}B 3QMAS NMR spectra for Na_2O-B_2O_3 glasses. The ^{11}B NMR spectra of $NaAlSiO_4$-$NaBSiO_4$ and $NaAlSi_3O_8$-$NaBSi_3O_8$ glasses show that $^{[4]}B$ increases as boron content increases while non-ring ($^{[3]}B$) decreases. ^{27}Al MAS NMR spectra for $NaAlSiO_4$-$NaBSiO_4$ glasses confirm that four-coordinated aluminum ($^{[4]}Al$) is dominant. It is also observed that a drastic decrease in the

peak widths (full-width at half-maximum, FWHM) of $^{[4]}$Al with an addition of boron into nepheline glasses, indicating a decrease in structural and topological disorder around $^{[4]}$Al. The quantitative atomic environments around boron of multicomponent glasses are estimated from the simulation results of ^{11}B MAS NMR spectra, revealing complex-nonlinear variation of boron topology with varying composition. ^{17}O MAS and 3QMAS NMR spectra for $NaAlSiO_4$-$NaBSiO_4$ glasses show that Na-O-Si, B-O-B, and B-O-Si increase with increasing boron content, indicating that a drastic increase in dissolution rate might be due to an increase in B-O-B and B-O-Si which are relatively weaker bridging oxygen (BOs). An increase in non-bridging oxygen (NBO), Na-O-Si, implying a decrease in the degree of polymerization can explain the low viscosity of boron-bearing silicate melts. Na-O-B is firstly observed in ^{17}O 3QMAS NMR spectra for $NaAl_{0.25}B_{0.75}SiO_4$ glasses. The current experimental results with the changes in coordination environment, topological structure, and network connectivity in the nepheline-malinkoite and albite-reedmergnerite glasses can improve understanding of the structure-property relationships including dissolution and viscosity of multicomponent boron-bearing silicate melts.

Key words: Sodium borate glasses, boron-bearing multicomponent silicate melts (nepheline-malinkoite and albite-reedmergnerite pseudo-binary glasses), NMR, atomic structure

Table of Contents

List of Figures

Figure 8. Total isotropic projections of ^{27}Al 3QMAS NMR spectra for $NaAlSiO_4$-$NaBSiO_4$ glasses with varying X_{Ma}.

Figure 9. ^{17}O MAS NMR spectra for $NaAlSiO_4$-$NaBSiO_4$ glasses at 9.4 T with varying X_{Ma}.

Figure 10. ^{17}O 3QMAS NMR spectra for $NaAlSiO_4$-$NaBSiO_4$ glasses at 9.4 T with varying X_{Ma}. Contour lines of the spectra with X_{Ma}=0 are drawn at 5% intervals from relative intensities of 13~88% with added lines at 1%, 3%, 6%, and 9%. Contour lines of the spectra with X_{Ma}=0.25 and 0.50 are drawn at 5% intervals from relative intensities of 13~88% with added lines at 1.5%, 3%, 6%, and 9%. Contour lines of the spectra with X_{Ma}=0.75 are drawn at 5% intervals from relative intensities of 13~93% with added lines at 1.5%, 5%, and 8%. Contour lines of the spectra with X_{Ma}=1 are drawn at 5% intervals from relative intensities of 13~93% with added lines at 3%, 8%, and 8%.

Figure 11. Total isotropic projections of ^{17}O 3QMAS NMR spectra for $NaAlSiO_4$-$NaBSiO_4$ glasses with varying X_{Ma}.

Figure 12. ^{11}B MAS NMR spectra for $NaAlSi_3O_8$-$NaBSi_3O_8$ glasses at 9.4 T with varying mole fraction of reedmergnerite component [X_{Rd}=$NaBSi_3O_8$/($NaBSi_3O_8$+$NaAlSi_3O_8$)].

Figure 13. The population of boron species from ^{11}B MAS NMR spectra for $NaAlSi_3O_8$-$NaBSi_3O_8$ glasses with varying X_{Rd}. The blue and red circles refer to the population of ring ($^{[3]}B$) and non-ring ($^{[3]}B$), respectively. The green square refers to the population of $^{[4]}B$. Error bar was estimated from the uncertainty in sample composition, phasing of NMR spectrum, and NMR processing conditions.

Figure 14. ^{11}B MAS NMR spectra for $NaAlSiO_4$-$NaBSiO_4$ (black) and $NaAlSi_3O_8$-$NaBSi_3O_8$ (red) glasses at 9.4 T with the same B/(B+Al) ratio, 0.25 and 1.

Figure 15. The population of boron species from ^{11}B MAS NMR spectra for $NaAlSiO_4$-$NaBSiO_4$ (black) and $NaAlSi_3O_8$-$NaBSi_3O_8$ (red) glasses with varying B/(B+Al) ratio.

Figure 16. The schematic diagram of the atomic configuration of $NaAlSiO_4$-$NaBSiO_4$ glasses with varying B/(B+Al) ratio.

Appendix

Figure A1. Optimized geometries of $^{[3]}BO_3$[xNa, (3-x)H] and $^{[3]}BO_3$[xNa, (3-x)$^{[3]}B(OH)_2$] clusters with the number of Na (x) at the B3LYP/6-311+(2d,p) level of theory. A~D show the optimized geometries of $^{[3]}BO_3$[xNa, (3-x)H] with x=0, 1, 2, 3. F~H show the optimized geometries of $^{[3]}BO_3$[xNa, (3-x)$^{[3]}B(OH)_2$] with x=0, 1, 2, 3. The atoms in order of decreasing size are Na, B, O, and H. Bond lengths and angles are given in Table A1.

Figure A2. The ^{11}B isotropic chemical shielding of $^{[3]}BO_3$[xNa, (3-x)H] clusters with the number of Na (x).

Figure A3. The ^{11}B isotropic chemical shielding of $^{[3]}BO_3$[xNa, (3-x)$^{[3]}B(OH)_2$] clusters with the number of Na (x).

Figure A4. The simulation results, where thin black, red, and green lines refer total simulations, non-ring ($^{[3]}B$) species, and $^{[4]}B$ species, respectively, and ^{11}B MAS NMR spectrum (bold black line) for $NaAlSiO_4$-$NaBSiO_4$ glasses with X_{Ma}=0.25 (A), 0.50 (B), 0.75 (C), and 1 (D).

Figure A5. The simulation results, where thin black, blue, red, and green lines refer total simulations, ring ($^{[3]}B$) species, non-ring ($^{[3]}B$) species, and $^{[4]}B$ species, respectively, and ^{11}B MAS NMR spectrum (bold black line) for $NaAlSi_3O_8$-$NaBSi_3O_8$ glasses with X_{Rd}=0.25 (A), 0.50 (B), 0.75 (C), and 1 (D).

Figure A6. The FWHM results with varying X_{Ma} from ^{27}Al MAS NMR spectra for $NaAlSiO_4$-$NaBSiO_4$ glasses.

Figure A7. The FWHM results with varying X_{Ma} from MAS dimension of ^{27}Al 3QMAS NMR spectra for $NaAlSiO_4$-$NaBSiO_4$ glasses.

Figure A8. The FWHM results with varying X_{Ma} from isotropic dimension of ^{27}Al 3QMAS NMR spectra for $NaAlSiO_4$-$NaBSiO_4$ glasses.

List of Tables

Appendix

1. INTRODUCTION

Boron is a trace element, which is contained about 10-11 ppm in the continental crust, 1.8 ppm in the oceanic crust, and 0.1-0.8 ppm in the primitive mantle (Lodders and Fegley, 1998; Lyubetskaya and Korenaga, 2007; Palme and O'Neill, 2003; Rudnick and Gao, 2003; Taylor and McLennan, 1995; Wedepohl, 1995; White and Klein, 2014). In spite of its low abundance, its application to geological processes is important because a small amount of boron leads a significant change in transport properties, such as viscosity and dissolution rate. The viscosity of magma affects the generation, migration, and eruption of magma. Boron-bearing magma erupts less explosively than boron-free magma because boron lowers viscosity. For example, a few weight percent of boron can lower the viscosity of granitic magmas to two orders of magnitude at 750 °C at which the crystallization of granitic rock from melts begins, hence it facilitates the movement of the magma (Dingwell et al., 1992). The partitioning of boron into melts is favored than into solids, and this characteristic is called incompatibility. Therefore, the concentration of boron can be higher in fractionated silicate melts. For example, it can be up to 1 wt% B_2O_3 in pegmatitic melts. A recent study reported that the viscosity of pegmatitic melts decreases to a fifth its original value with approximately 1 wt% B_2O_3 (Bartels et al., 2013). In addition, because the crust recycling has been studied by the adsorption and leaching of boron in oceanic crust with contact with seawater, the mechanism of the weathering process has been of interest to geochemists.

These weathering process related with water-melt interaction is also considered crucial in environmental sciences and industrial glass society. A nuclear waste glasses include approximately 5 wt% B_2O_3, because boron is one of the best glass-forming cation facilitating a manufacturing process of them. Though the use of boron reduces the cost of manufacturing the glasses, it also makes them weaker. Therefore, there are a lot of studies of the stability related with boron of the nuclear waste glasses (Dhara et al., 2016; Gin et al., 2013; Hopf et al., 2016a; McCloy et al., 2015; Nicoleau et al., 2015; Pierce et al., 2010; Rajmohan et al., 2010). The reactivity and corrosion of pristine glasses before alteration with varying composition are essential to model the dissolution mechanism. A dissolution of elements composing the nuclear waste glasses measure the degree of corrosion of the glasses. Aluminum is also used to make the nuclear waste glasses, and because boron and aluminum are both network-former and trivalent cation, the mixing and element

interactions between them need to be constrained to understand the dissolution mechanism. A study of the dissolution rate of $NaAlSiO_4$-$NaBSiO_4$ glasses with varying B/Al ratio reported an increase in the dissolution rate of boron from ~$10^{-8.8}$ mol/m^2s ($NaAl_{0.25}B_{0.75}SiO_4$ glasses, X_B [=B/(B+Al)]=0.75) to ~$10^{-6.0}$ mol/m^2s ($NaAl_{0.20}B_{0.80}SiO_4$ glasses, X_B=0.80) (Pierce et al., 2010).

Boron has various atomic structure with temperature, composition, and pressure. For example, there are two coordination states of boron at ambient pressure: three-coordinated boron ($^{[3]}$B) and four-coordinated boron ($^{[4]}$B). There are two topological species of $^{[3]}$B: ring ($^{[3]}$B) and non-ring ($^{[3]}$B). When all $^{[3]}$B are connected forming ring shape, it is called ring ($^{[3]}$B). When the linkage of $^{[3]}$B does not form ring shape, it is called non-ring ($^{[3]}$B). There have been a lot of studies which investigate the atomic structure of boron-bearing melts not only with varying composition but also with varying pressure using nuclear magnetic resonance (NMR) and inelastic X-ray scattering method (Du and Stebbins, 2003a, b; Hopf et al., 2016b; Lee et al., 2005a; Lee et al., 2007; Lee et al., 2005b; Lee et al., 2001; Lee and Stebbins, 2002; Pierce et al., 2010). It is well known that $^{[4]}$B increases with increasing alkali content in alkali borate glasses, but the change in topological species of $^{[3]}$B still remains unsolved. It is because there are some discrepancy between experimental and computer simulation results (see Appendix A1 for more details). For borosilicate glasses, which are composed of both network forming cations, ring and non-ring ($^{[3]}$B) peaks are well resolved in ^{11}B 3QMAS NMR spectra at 14.1 T, and non-ring ($^{[3]}$B) increases at the expense of ring ($^{[3]}$B) with increasing Si/B ratio (Lee and Stebbins, 2002).

The aforementioned transport properties of boron-bearing silicate melts are dependent on composition, pressure, and temperature. It is well known that these variables affect the atomic structure of the glasses. Therefore, the detailed information on atomic structure of glasses is a key to understanding the change in macroscopic properties of the glasses, such as energy, entropy, viscosity, and diffusivity. For example, it is well established that the viscosity of silicate glasses and melts is dependent on the degree of polymerization (Giordano and Dingwell, 2003b). Because the degree of polymerization can be provided by oxygen environment, non-bridging oxygen (NBO) fraction, the viscosity of silicate glasses and melts exponentially decreases with increasing NBO fraction, which has weaker bonding than bridging oxygen (BO) (Lee, 2005; Stebbins and Xu, 1997). The detailed information on the network connectivity between framework cations can be obtained from ^{17}O nuclear

magnetic resonance (NMR) spectroscopy. According to Stokes-Einstein relations that the viscosity is inversely proportional to diffusivity, the atomistic origin of diffusivity can be also explained by network connectivity of silicate melts based on oxygen configurations.

There have been a lot of study focusing on the dissolution mechanism with varying pH condition of solutions, but there lacks of studies that focus on the effect of atomic structure on dissolution with varying composition. The previous study suggested that the drastic increase in dissolution rate of boron in $NaAlSiO_4$-$NaBSiO_4$ glasses is attributed to a sudden decrease of non-ring species of three-coordinated boron [non-ring ($^{[3]}$B)] based on ^{11}B NMR spectroscopy (Pierce et al., 2010). However, it has been reported that the assignment of ring and non-ring structure of $^{[3]}$B is uncertain, thus there can be some ambiguity in their peak assignment of ^{11}B NMR results (see Section 2.3 for more details). The dissolution of an element from solid to liquid phase is accompanied by breaking weaker bond linkage. Because the contribution to change in dissolution rate from medium-range structure (i.e., NBOs and BOs) is bigger than that from short-range structure (i.e., coordination number), it is needed to explore the oxygen configuration of the glasses to provide insights into the dissolution mechanism with varying boron content. However, there are no experimental results about the network connectivity of the glasses with varying boron content.

The powerful tool to investigate the network connectivity is ^{17}O NMR spectroscopy. There has been a lot of studies which provide the network connectivity of silicate glasses including multicomponent silicate glasses, such as glasses in diopside-Ca-tschermakite join and in jadeite-diopside join (Park and Lee, 2012; Park and Lee, 2014). The study of suggested that NBO preference between Ca-NBO and Mg-NBO partially explains the dissolution mechanism of basalts in contact with aqueous solutions from the fact that Mg-NBO is stronger bond than Ca-NBO based on ^{17}O NMR spectroscopy (Park and Lee, 2012). In $NaAlSiO_4$-$NaBSiO_4$ glasses, there can be one candidate of NBO with boron, i.e., Na-O-B and three candidates of BOs with boron, i.e., B-O-B, B-O-Si, and B-O-Al. If Na-O-B fraction increases with increasing boron content, the increase in dissolution rate of boron could be due to the breakage of weaker Na-O-B bond. If there are few Na-O-B in the glasses, the change in dissolution of boron could be attributed to the breakage of B-O-B and B-O-Si which are weak BOs. However, there are no experimental results which show the presence of Na-O-B and oxygen configurations in $NaAlSiO_4$-$NaBSiO_4$ glasses with varying composition. Thus, the detailed information on network connectivity of the glasses with

varying boron content needs to be provided to establish the relationship between the atomic structure and transport properties including dissolution rate and viscosity.

In this study, we explore the atomic structure of boron of Na_2O-B_2O_3 glasses with varying sodium content based on the peak assignment from the quantum chemical calculations. We also explore the atomic environments (i.e., coordination environment and topological distributions), extent of disorder, and network connectivity of multicomponent boron-bearing nepheline melts ($NaAlSiO_4$-$NaBSiO_4$) using multi-nuclear (^{11}B, ^{27}Al, and ^{17}O) high-resolution solid-state NMR and propose the partial dissolution mechanism of boron-bearing sodium-aluminosilicate glasses based on network connectivity from ^{11}B and ^{17}O NMR results.

2. EXPERIMENTAL METHOD

2.1. Sample preparation

Na_2O-B_2O_3 glasses. A series of glasses in Na_2O-B_2O_3 system containing 0, 14, 20, and 33 mol% Na_2O component were synthesized from carbonate (Na_2CO_3) and oxide glasses (B_2O_3). The starting Na_2CO_3 powders were dried at 400 ^oC for 48h; B_2O_3 glasses were synthesized by fusing boric acid (H_3BO_3) with a torch. The B_2O_3 melt was quenched by removing the Pt crucible from a torch for 5 times and then grinded to be powders. The weighed powders were mixed by grinding in an agate mortar, and then decarbonated in a Pt crucible at 800 ^oC for 30 min. The samples were then melted above their respective melting temperature (950 ^oC) for 30 min, and quenched into glasses by plunging the bottom of the Pt crucible into a water bath. Approximately 0.2 wt% of cobalt oxide was added, except for B_2O_3 glasses, to enhance spin-lattice relaxation. Table 1 shows the nominal and chemical compositions determined by inductively coupled plasma-atomic emission spectroscopy (ICP-AES) for Na_2O-B_2O_3 glasses with varying the mole fraction of Na [X_{Na}=Na/(Na+B)].

$NaAlSiO_4$-$NaBSiO_4$ glasses. A series of glasses in the nepheline ($NaAlSiO_4$) – malinkoite ($NaBSiO_4$) pseudo-binary join containing 0, 25, 50, 75, and 100 mol% $NaBSiO_4$ component were synthesized from carbonate (Na_2CO_3) and oxides (Na_2O, Al_2O_3, B_2O_3, and SiO_2). The staring Na_2CO_3, Al_2O_3, and SiO_2 powders were dried at 400 ^oC for 48 h; B_2O_3 glasses were synthesized by fusing boric acid (H_3BO_3) with a torch. The B_2O_3 melt was quenched by removing the Pt crucible from a torch for 5 times and then grinded to be powders. The weighed powders were mixed by grinding in an agate mortar, and then decarbonated in a Pt crucible at 800 ^oC for 30 min. The samples were then melted above their respective melting temperature (950-1600 ^oC) for 30 min, and quenched into glasses by plunging the bottom of the Pt crucible into a water bath. Approximately 0.2 wt% of cobalt oxide was added to enhance spin-lattice relaxation. ^{17}O-enriched $NaAlSiO_4$-$NaBSiO_4$ glasses were synthesized from carbonates and oxides, including ^{17}O-enriched SiO_2. The ^{17}O-enriched SiO_2 was prepared by hydrolyzing $SiCl_4$ in 40% ^{17}O-enriched water. Approximately 0.2 wt% of cobalt oxide was added to enhance spin-lattice relaxation. The mixtures were then fused in a Pt crucible for 10 min above melting temperature (950-1600 ^oC) in an Ar environment. The melts were quenched by removing the crucible from the furnace and then manually

lowering it into water. Table 2 and 3 show the nominal compositions and chemical compositions determined by ICP-AES for glasses without enrichment of ^{17}O and ^{17}O enriched glasses in the $NaAlSiO_4$-$NaBSiO_4$ pseudo-binary system, respectively.

$NaAlSi_3O_8$-$NaBSi_3O_8$ glasses. A series of glasses in the albite ($NaAlSi_3O_8$) – reedmergnerite ($NaBSi_3O_8$) pseudo-binary join containing 0, 25, 50, 75, and 100 mol% $NaBSi_3O_8$ component were synthesized from carbonate (Na_2CO_3) and oxides (Na_2O, Al_2O_3, B_2O_3, and SiO_2). The staring Na_2CO_3, Al_2O_3, and SiO_2 powders were dried at 400 ^oC for 48 h; B_2O_3 glasses were synthesized by fusing boric acid (H_3BO_3) with a torch. The B_2O_3 melt was quenched by removing the Pt crucible from a torch for 5 times and then grinded to be powders. The weighed powders were mixed by grinding in an agate mortar, and then decarbonated in a Pt crucible at 800 ^oC for 30 min. The samples were then melted above their respective melting temperature (950-1600 ^oC) for 30 min, and quenched into glasses by plunging the bottom of the Pt crucible into a water bath. Approximately 0.2 wt% of cobalt oxide was added to enhance spin-lattice relaxation. Table 4 shows the nominal compositions of $NaAlSi_3O_8$-$NaBSi_3O_8$ glasses.

Table 1. Nominal compositions (weight %) and ICP analyses of glasses in the Na_2O-B_2O_3 system. X_{Na} is the mole fraction of Na.

Composition		wt% (nominal composition)		wt% (ICP analysis)	
		Na_2O	B_2O_3	Na_2O	B_2O_3
X_{Na}	0	0	100	-	-
	0.14	12.9	87.1	12.30	87.70
	0.20	18.2	81.8	17.51	82.49
	0.33	30.8	69.2	28.99	71.01

Table 2. Nominal compositions (weight %) and ICP analyses of $NaAlSiO_4$-$NaBSiO_4$ glasses. X_{Ma} is the mole fraction of malinkoite component.

Composition		wt% (nominal composition)			
		Na_2O	Al_2O_3	B_2O_3	SiO_2
X_{Ma}	0	21.82	35.89	0	42.30
	0.25	22.45	27.70	6.31	43.54
	0.50	23.13	19.03	12.99	44.85
	0.75	23.85	9.81	20.09	46.24
	1	24.62	0	27.65	47.73

Composition		wt% (nominal composition)			wt% (ICP analysis)[a]		
		Na_2O	Al_2O_3	B_2O_3	Na_2O	Al_2O_3	B_2O_3
X_{Ma}	0	37.81	62.19	0	39.35	60.23	0.4
	0.25	39.76	49.06	11.18	41.17	47.29	11.55
	0.50	41.94	34.51	23.55	42.70	32.86	24.44
	0.75	44.37	18.25	37.38	45.31	17.38	37.30
	1	47.10	0	52.90	46.47	0.3	53.21

[a] The analysis was performed for Na_2O, Al_2O_3, and B_2O_3 because SiO_2 is volatilized during pretreatment by reacting with hydrofluoric acid. The chemical analysis here assumes that the nominal SiO_2 content is correct.

Table 3. Nominal compositions (weight %) and ICP analyses of ^{17}O enriched $NaAlSiO_4$-$NaBSiO_4$ glasses. X_{Ma} is the mole fraction of malinkoite component.

Composition		wt% (nominal composition)						
		Na_2O	Al_2O_3	B_2O_3	SiO_2			
X_{Ma}	0	21.63	35.59	0	42.78			
	0.25	22.26	27.47	6.25	44.02			
	0.50	22.93	18.86	12.88	45.34			
	0.75	23.63	9.72	19.91	46.74			
	1	24.39	0	27.39	48.22			
Composition		wt% (nominal composition)				wt% (ICP analysis)[a]		
		Na_2O	Al_2O_3	B_2O_3		Na_2O	Al_2O_3	B_2O_3
X_{Ma}	0	37.80	62.20	0		39.08	60.76	0.2
	0.25	39.76	49.07	11.16		40.84	47.14	12.02
	0.50	41.94	34.50	23.56		42.90	32.88	24.22
	0.75	44.37	18.25	37.38		44.09	17.50	38.41
	1	47.10	0	52.90		46.25	0.4	53.31

[a] The analysis was performed for Na_2O, Al_2O_3, and B_2O_3 because SiO_2 is volatilized during pretreatment by reacting with hydrofluoric acid. The chemical analysis here assumes that the nominal SiO_2 content is correct.

Table 4. Nominal compositions (weight %) of $NaAlSi_3O_8$-$NaBSi_3O_8$ glasses. X_{Rd} is the mole fraction of reedmergnerite component.

Composition		wt% (nominal composition)			
		Na_2O	Al_2O_3	B_2O_3	SiO_2
X_{Rd}	0	11.82	19.44	0	68.74
	0.25	12.00	14.81	3.37	69.82
	0.50	12.19	10.03	6.85	70.93
	0.75	12.39	5.10	10.44	72.07
	1	12.59	0	14.15	73.26

2.2. Previous peak assignment of non-ring species in ^{11}B NMR spectrum

Even though the NMR is a useful tool to investigate the atomic structure of boron which can resolve even topological species of $[3]B$, there are a fundamental problems of assigning peak of non-ring ($[3]B$) in ^{11}B MAS NMR spectra for the glasses which contain non-framework cations like Na. The peak assignment of boron species has been debated using computer simulation because ring ($[3]B$) is very unstable and thus cannot be generated, which is the cause of the differences between the results of quantum chemical calculations and experimental measurements. Even for the simplest B_2O_3 glasses at 1 atm, previous studies have reported that there are ~75% and ~30% of ring ($[3]B$) using NMR spectroscopy and molecular dynamic simulations, respectively (Bray, 1985b; Du and Stebbins, 2003a, b; Ferlat et al., 2008; Hwang et al., 1997; Lee et al., 2001). It was also suggested that the underestimated fraction of ring ($[3]B$) from calculations might be due to the unrealistically high quench rate using computer simulation, which cannot be produced in experimental method, implying that the fundamental problem of computer simulation not to form ring ($[3]B$) still remains to be solved (Kilymis et al., 2016).

Previous studies about atomic structure of boron in alkali borate glasses have followed the peak assignment of B_2O_3-SiO_2 glasses, which is not the case for alkali borate glasses which are composed of network modifying and network forming cations. Because there is a possibility that the presence of network modifying cation like Na affects ^{11}B NMR chemical shift of non-ring ($[3]B$), it is essential to re-assigning the boron environment of ^{11}B NMR spectra in case the system contains network modifying cations.

2.3. Spectrometer

The ^{11}B MAS and 3QMAS NMR spectra for Na_2O-B_2O_3, $NaAlSiO_4$-$NaBSiO_4$, and $NaAlSi_3O_8$-$NaBSi_3O_8$ glasses were collected using a Varian solid-state NMR 400 system (9.4 T) at a Larmor frequency of 128.34 MHz with a 3.2 mm Varian double-resonance probe (Seoul National University, Korea). A relaxation delay for ^{11}B MAS NMR was 1 s, and the radio frequency pulse strength was 0.2 μm. Approximately 96-288 scans of free-induction decay (FID) were averaged to achieve S/N ratio shown in the ^{11}B MAS NMR spectra. In the 3QMAS NMR experiment at 9.4 T, a fast amplitude modulation (FAM)-based shifted-echo

pulse sequence with a hard pulse of duration 4.3 μm for multiple-quantum excitation and two 1.9 μm pulses for single quantum reconversion, a soft pulse of duration 21 μm, and an echo time of approximately 300 μm (integer multiple of a rotor period) was used with a relaxation delay of 1 s. Approximately 96-288 scans of free-induction decay (FID) were averaged to achieve S/N ratio shown in the ^{11}B 3QMAS NMR spectra. The spectra were referenced to liquid boric acid (H_3BO_3), whose resonance was located at 19.6 ppm. The ^{27}Al MAS and 3QMAS NMR spectra for $NaAlSiO_4$-$NaBSiO_4$ were collected using a Varian solid-state NMR 400 system (9.4 T) at a Larmor frequency of 104.23 MHz with a 3.2 mm Varian double-resonance probe. A relaxation delay for ^{27}Al MAS NMR were 1 s and the radio frequency pulse strength was 0.3 μm. Approximately 960-1920 scans of FID were averaged to achieve the S/N ratio shown in the ^{27}Al MAS NMR spectra. In the 3QMAS NMR experiment at 9.4 T, FAM-based shifted-echo pulse sequence with a hard pulse of duration 3.0 μm for multiple-quantum excitation and two 0.7 μm pulses for single quantum reconversion, a soft pulse of duration 15 μm, and an echo time of approximately 500 μm (integer multiple of a rotor period) was used with a relaxation delay of 1 s. Approximately 1248-2880 scans of FID were averaged to achieve the S/N ratio shown in the ^{27}Al 3QMAS NMR spectra. The spectra were referenced to liquid aluminum chloride ($AlCl_3$). The ^{17}O 3QMAS NMR spectra for $NaAlSiO_4$-$NaBSiO_4$ glasses were collected using a Varian solid-state NMR 400 system (9.4 T) at a Larmor frequency of 54.23 MHz with a 4 mm Doty double-resonance probe. A FAM-based shifted-echo pulse sequence with a hard pulse of duration 4.5 μm for multiple-quantum excitation and two 1.1 μm pulses for single quantum reconversion, a soft pulse of duration 19.5 μm, and an echo time of approximately 357 μm (integer multiple of a rotor period) was used with a relaxation delay of 1 s. Approximately 4800-5760 scans of FID were averaged to achieve the S/N ratio shown in the ^{17}O 3QMAS NMR spectra. The spectra were referenced to external tap water.

3. RESULTS

3.1. Effects of Na on ^{11}B NMR chemical shift of non-ring ($^{[3]}$B) in Na_2O-B_2O_3 glasses and melts: A view from ^{11}B MAS and 3QMAS NMR results and quantum chemical calculations

Fig. 1A shows ^{11}B MAS NMR spectra for Na_2O-B_2O_3 glasses quenched from melts with varying X_{Na} [=Na/(Na+B)]. The spectrum for B_2O_3 glasses with X_{Na}=0 shows a quadupolar shape and is not very broad even though it is of amorphous materials, indicating that B_2O_3 glasses have less disorder in the atomic structures, consistent with the previous NMR study of B_2O_3 glasses (Bray, 1985a; Kriz and Bray, 1971; Lee et al., 2005a). The peak marked by red arrow in Fig. 1A indicates non-ring ($^{[3]}$B) species. Although the peaks of $^{[3]}$B and $^{[4]}$B are not fully resolved in ^{11}B MAS NMR spectra due to the low external magnetic field of NMR (9.4 T), the spectra shows that $^{[4]}$B (approximately -5~10 ppm) increases with increasing X_{Na}. The ^{11}B MAS NMR spectra for alkali borosilicate glasses were previously interpreted as $^{[4]}$B (approximately -5~10 ppm) increases at the expense of $^{[3]}$B (approximately -10~10 ppm and -5~20 ppm for non-ring and ring structure, respectively) with increasing alkali content (Du and Stebbins, 2003c; Pierce et al., 2010). This study, however, suggests that ^{11}B NMR chemical shift of non-ring ($^{[3]}$B) species can change with varying sodium content from the results of quantum chemical calculations indicating the peak of non-ring ($^{[3]}$B) can overlap with the peak of ring ($^{[3]}$B) (see Appendix 1 for more details). According to this peak assignment, the ^{11}B NMR spectra are interpreted as $^{[4]}$B increases at the expense of ring ($^{[3]}$B), and non-ring ($^{[3]}$B) does not change with increasing X_{Na}. Fig. 1B shows 2D ^{11}B 3QMAS NMR spectra for Na_2O-B_2O_3 glasses quenched from melts with varying X_{Na}=0, 0.14, and 0.20. Two B-coordination environments (i.e., $^{[3]}$B and $^{[4]}$B) and topological species of $^{[3]}$B (i.e., ring and non-ring species) are well resolved. There is only $^{[3]}$B in the ^{11}B 3MQAS NMR spectrum for B_2O_3 glasses, consistent with the results of ^{11}B MAS NMR spectrum. It is observed that $^{[4]}$B increases with increasing sodium content at the expense of ring ($^{[3]}$B), consistent with ^{11}B MAS NMR spectra. The total isotropic projections of ^{11}B 3QMAS NMR spectra and simulation results for Na_2O-B_2O_3 glasses at X_{Na}=0 and 0.14 quenched from melts with varying X_{Na} are shown in Fig. 1C. Based on the new interpretation of a change in ^{11}B NMR chemical shift of non-ring ($^{[3]}$B), $^{[4]}$B (green line) increases at the expense of ring (blue line), and non-ring (red line) peak shifts to higher frequency with increasing X_{Na}.

The two topological species of $^{[4]}$B (approximately -2~2 ppm in MAS dimension and 0~7.5 ppm in isotropic dimension) are firstly observed in ^{11}B 3QMAS NMR spectra for X_{Na}=0.14 glasses, although they are not clearly observed in the MAS and isotropic dimension because of overlapping two peaks. For the spectra with X_{Na} larger than 0.20, there is only one topological species of $^{[4]}$B in the ^{11}B 3QMAS NMR spectra. In this study, the narrow (blue shaded) and broad (red shaded) peaks are assigned as $^{[4]}$B-a (approximately -3~3 ppm in MAS dimension and -5~5 ppm in isotropic dimension) and $^{[4]}$B-b (approximately -5~2 ppm in MAS dimension and -2~5 ppm in isotropic dimension), respectively. Previous study observed that two topological species of $^{[4]}$B of B_2O_3 glasses at high pressure using ^{11}B NMR spectroscopy at 14.1 T (Lee et al., 2005b). They assigned $^{[4]}$B-a (approximately -1~2 ppm in MAS dimension and 0~6 ppm in isotropic dimension) as $^{[4]}$B with next nearest neighbors of ring or non-ring ($^{[3]}$B) and $^{[4]}$B-b (-4~0 ppm in MAS dimension and -5~5 ppm in isotropic dimension) as $^{[4]}$B with next nearest neighbors of non-ring ($^{[3]}$B). Based on the peak assignment of previous study, the narrow $^{[4]}$B-a site has non-ring ($^{[3]}$B) or $^{[4]}$B as next nearest neighbors, which is similar with the $^{[4]}$B-b of previous study, and the broad $^{[4]}$B-b site has ring ($^{[3]}$B) as next nearest neighbors, which is similar with the $^{[4]}$B-a of previous study. It should be noted that the two topological species of $^{[4]}$B of the previous study are pressure-induced, which is not the case of in current composition-induced results. Fig. 1D shows the schematic diagram for the two topological species of $^{[4]}$B which have different spatial proximity of ring or non-ring ($^{[3]}$B) species. The top cluster presents the $^{[4]}$B-a site with non-ring ($^{[3]}$B) or $^{[4]}$B as nearest neighbors. The bottom cluster presents the $^{[4]}$B-b site with ring ($^{[3]}$B) as nearest neighbors.

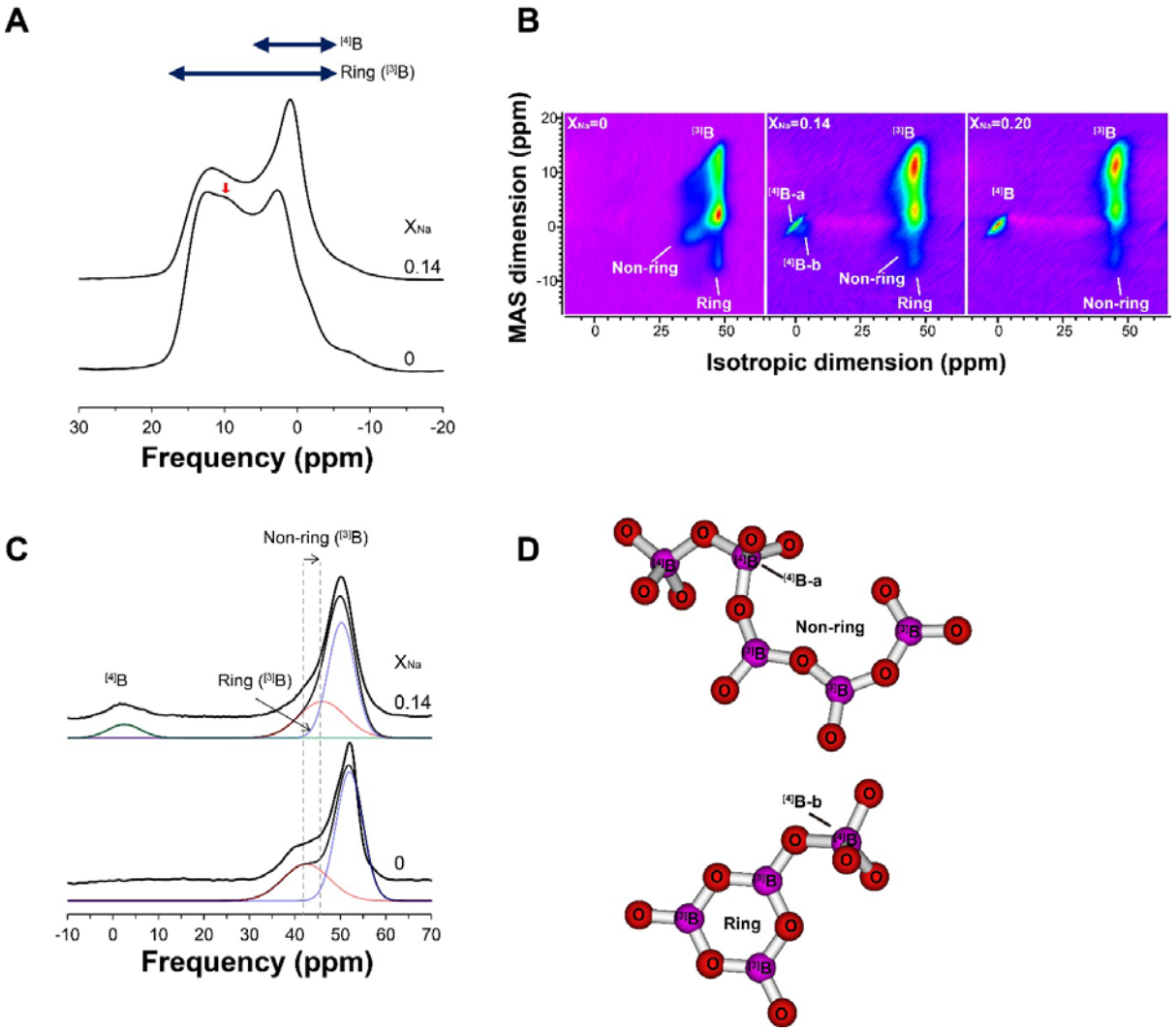

Figure 1. (A) ^{11}B MAS NMR spectra for Na_2O-B_2O_3 glasses at 9.4 T with varying mole fraction of Na [X_{Na}=Na/(Na+B)]. (B) ^{11}B 3QMAS NMR spectra for Na_2O-B_2O_3 glasses at 9.4 T with varying X_{Na}=0, 0.14, and 0.20. (C) The total isotropic projections of ^{11}B 3QMAS NMR spectra (bold black line) for X_{Na}=0 and 0.14 and simulation results of the projection, where thin black, blue, red, and green lines refer total simulations, ring ([3]B) species, non-ring ([3]B) species, and [4]B species, respectively. (D) The schematic diagram for the two sites of [4]B which have different proximity of ring or non-ring ([3]B) species.

3.2. Effect of boron fraction [B/(B+Al)] on B coordination environments in boron-bearing nepheline ($NaAlSiO_4$-$NaBSiO_4$) glasses and melts: Insights from ^{11}B MAS and 3QMAS NMR results

Fig. 2 shows ^{11}B MAS NMR spectra for $NaAlSiO_4$-$NaBSiO_4$ glasses quenched from melts with varying X_{Ma} [=$NaBSiO_4$/($NaBSiO_4$+$NaAlSiO_4$)]. The ratio of Na/B+Na is 0.8 (X_{Ma}=0.25), 0.67 (X_{Ma}=0.50), 0.57 (X_{Ma}=0.75), and 0.5 (X_{Ma}=1) for each glass. Since there are no ring ($^{[3]}B$) species above X_{Na}=0.33 in Na_2O-B_2O_3 glasses in this study (Fig. 1A-B), it is assumed to be only non-ring ($^{[3]}B$) in the multicomponent glasses. As X_{Ma} increases from 0.25 to 1, $^{[4]}B$ increases and non-ring ($^{[3]}B$) decreases. Two boron coordination-environments are partially resolved in the ^{11}B MAS NMR spectra. Because it is assumed that there are only non-ring ($^{[3]}B$) species in $NaAlSiO_4$-$NaBSiO_4$ glasses, the simulation was performed with $^{[4]}B$ and non-ring ($^{[3]}B$) species using the software Dmfit with *Q MAS 1/2* function which is specialized at fitting quadrupolar nuclear like boron (Massiot et al., 2002). The population of boron species is shown in Fig. 3. Non-ring ($^{[3]}B$) decreases from ~50% to ~12% and $^{[4]}B$ increases from ~46% to ~88% as X_{Ma} increases. The simulation results were presented in Appendix A2. The previous study reported that there are more than 35% of ring ($^{[3]}B$) in $NaAlSiO_4$-$NaBSiO_4$ glasses (Pierce et al., 2010). However, there can be an uncertainty of fitting the ^{11}B MAS NMR spectra since *Gaussian* function was used to convolute the experimental data, which is not specialized at quadrupolar nuclear. In addition, there can be an ambiguity of peak assignment of non-ring ($^{[3]}B$) in ^{11}B NMR results for the glasses containing non-framework cations.

^{11}B 3QMAS NMR spectra for $NaAlSiO_4$-$NaBSiO_4$ glasses quenched from melts with varying X_{Ma} are shown in Fig. 4. The peaks of $^{[3]}B$ and $^{[4]}B$ are resolved in the ^{11}B 3QMAS NMR spectra. As X_{Ma} increases, $^{[4]}B$ increases at the expense of non-ring ($^{[3]}B$), which is consistent with ^{11}B MAS NMR results. There are only one topological species of $^{[4]}B$ in boron-bearing nepheline glasses. In Fig. 5, the total isotropic projections of ^{11}B 3QMAS NMR spectra for $NaAlSiO_4$-$NaBSiO_4$ glasses quenched from melts are shown. Non-ring ($^{[3]}B$) decreases and $^{[4]}B$ increases as X_{Ma} increases, which is consistent with the results from ^{11}B MAS NMR spectra in this study.

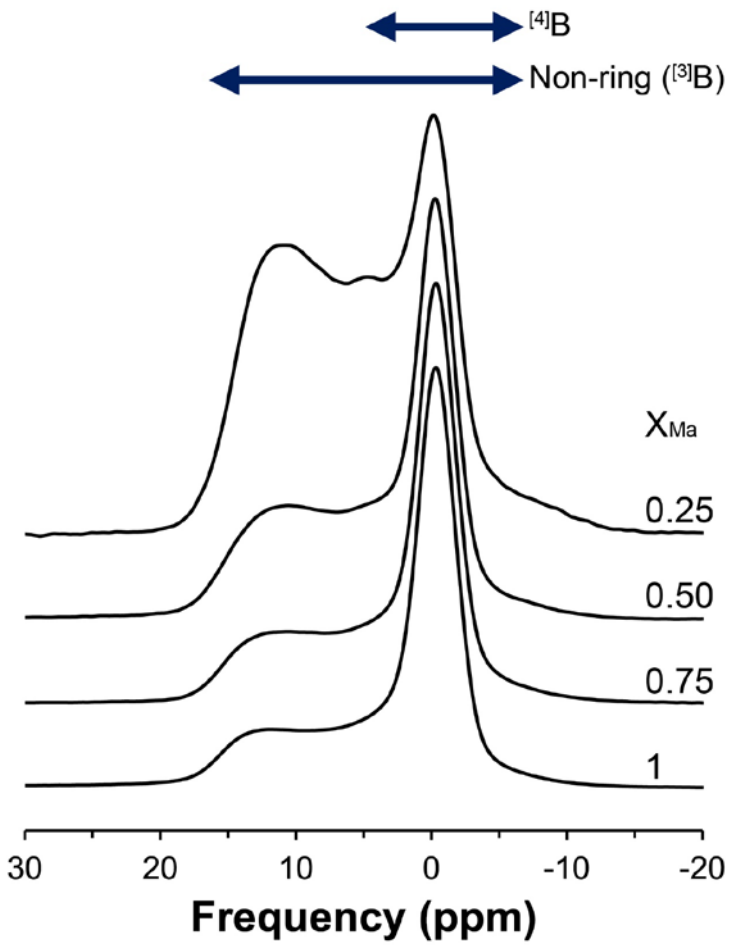

Figure 2. ^{11}B MAS NMR spectra for $NaAlSiO_4$-$NaBSiO_4$ glasses at 9.4 T with varying mole fraction of malinkoite component [X_{Ma}=$NaBSiO_4$/($NaBSiO_4$+$NaAlSiO_4$)].

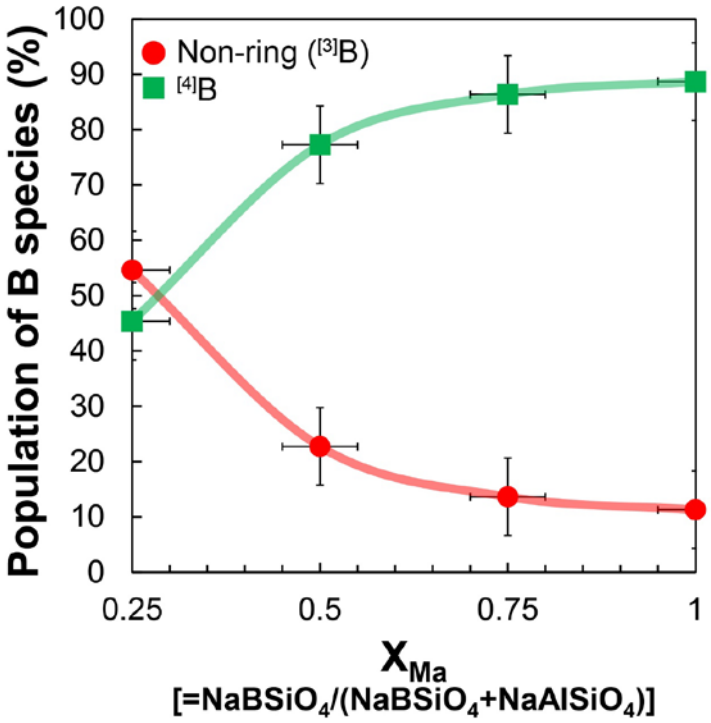

Figure 3. The population of boron species from ^{11}B MAS NMR spectra for $NaAlSiO_4$-$NaBSiO_4$ glasses with varying X_{Ma}. The blue and red circles refer to the population of ring ($^{[3]}$B) and non-ring ($^{[3]}$B), respectively. The green square refers to the population of $^{[4]}$B. Error bar was estimated from the uncertainty in sample composition, phasing of NMR spectrum, and NMR processing conditions.

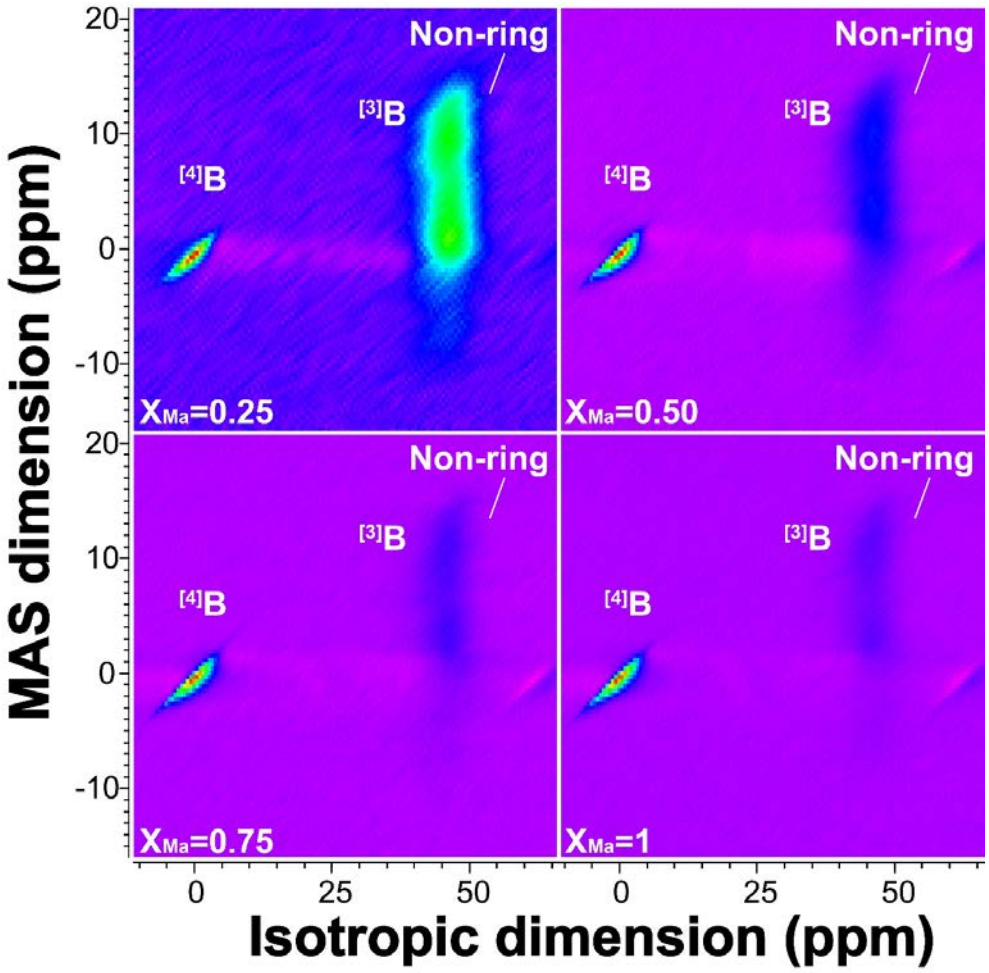

Figure 4. ^{11}B 3QMAS NMR spectra for $NaAlSiO_4$-$NaBSiO_4$ glasses at 9.4 T with varying X_{Ma}.

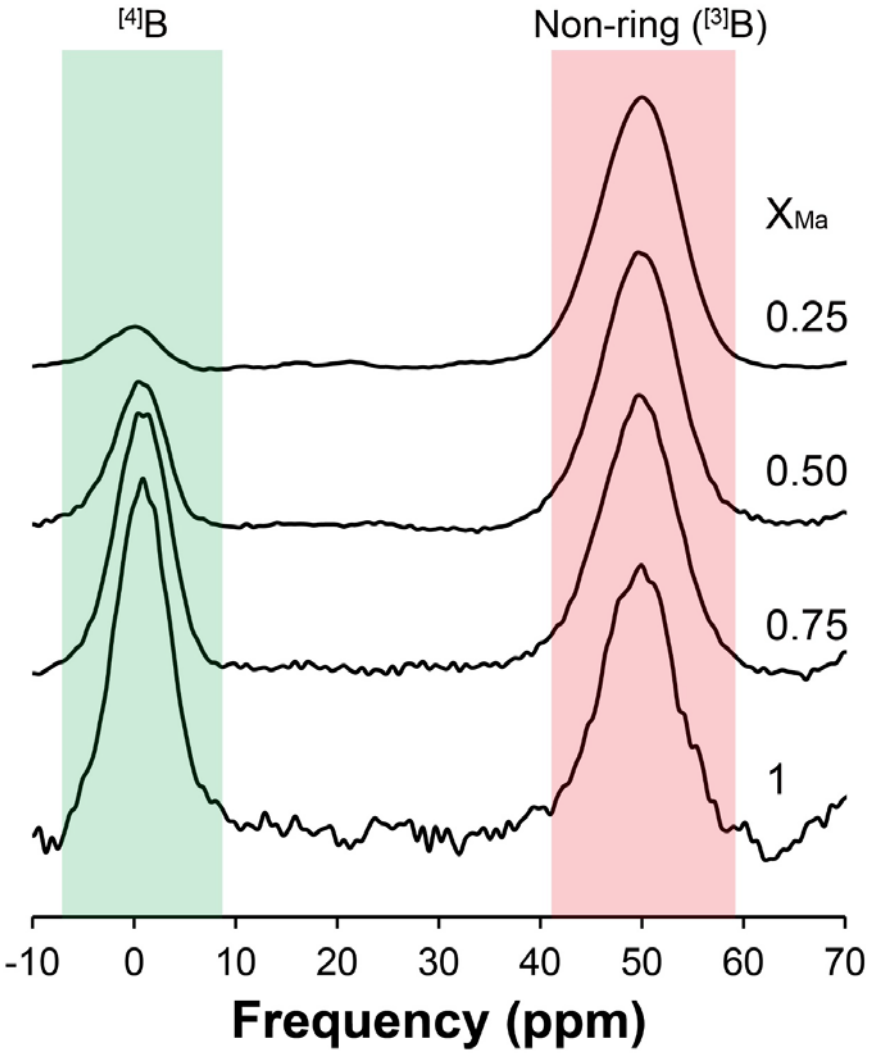

Figure 5. Total isotropic projections of ^{11}B 3QMAS NMR spectra for $NaAlSiO_4$-$NaBSiO_4$ glasses with varying X_{Ma}.

3.3. Effect of boron fraction [B/B+Al] on Al coordination environments in boron-bearing nepheline ($NaAlSiO_4$-$NaBSiO_4$) glasses and melts: Insights from ^{27}Al MAS and 3QMAS NMR results

Fig. 6 shows ^{27}Al MAS NMR spectra for $NaAlSiO_4$-$NaBSiO_4$ glasses quenched from melts with varying X_{Ma}. The dominant peak at ~48 ppm corresponds to four-coordinated Al ($^{[4]}$Al). The ^{27}Al chemical shifts of $^{[4]}$Al do not change with varying X_{Ma}. The peak shape with long tails extending toward lower chemical shift ranges indicates that there are a large degree of distribution of C_q (i.e., the quadrupolar coupling constant) and the isotropic chemical shift (i.e., δ_{iso}^{CS}) of $^{[4]}$Al environments, indicating a structural disorder in the glasses of interest. The peak widths of $^{[4]}$Al in the ^{27}Al MAS NMR spectra for the multicomponent glasses with X_{Ma}=0.25, 0.50, and 0.75 are much broader than the spectrum for the glasses without boron (i.e., $NaAlSiO_4$, X_{Ma}=0). While the peak widths (full-width at half-maximum, FWHM) of $NaAlSiO_4$ glasses with are approximately 27±0.5 ppm, those for boron-bearing glasses drastically decreases with X_{Ma}=0.25, approximately 21±1.0 ppm, and does not change as X_{Ma} increases from 0.25 to 0.75. The FWHM of $NaAlSiO_4$-$NaBSiO_4$ glasses for MAS and isotropic dimension with varying X_{Ma} are shown in Appendix A3. These results indicate that the degree of network distortion around the Al and/or configurational disorder of the $NaAlSiO_4$ glasses is much larger for the boron-bearing silicate glasses.

The ^{27}Al 3QMAS NMR spectra for $NaAlSiO_4$-$NaBSiO_4$ glasses quenched from melts with varying X_{Ma} are shown in Fig. 7 (top). While only $^{[4]}$Al is observed in the glasses with X_{Ma}=0, 0.25, and 0.50, which is consistent with the ^{27}Al MAS NMR spectra, a small but detectable $^{[5]}$Al is also observed for the glass at X_{Ma}=0.75 (~-22±1.5 ppm in the isotropic dimension) from the ^{27}Al 3QMAS NMR method. Fig. 7 (bottom) shows the effect of composition on the C_q [$=P_q/(1+\eta^2/3)^{1/2}$, where P_q and η are the quadrupolar coupling product and the asymmetry parameter assumed to be 0.5, respectively] of $^{[4]}$Al in the $NaAlSiO_4$-$NaBSiO_4$ glasses based on the previous study (Park and Lee, 2012). P_q was obtained from the center of gravity of the $^{[4]}$Al peak in the ^{27}Al 3QMAS NMR spectra. C_q is used to represent a degree of distortion and a deviation from perfect tetrahedral symmetry (e.g., $^{[4]}$Al) in the silicate glasses (Park and Lee, 2014). The C_q of $^{[4]}$Al in the glasses decreases from 5.07±0.2 MHz (X_{Ma}=0) to 4.45±0.2 MHz (X_{Ma}=0.25) with adding boron into $NaAlSiO_4$ glasses. The C_q (4.47±0.2 MHz) does not seem to be changed in the glasses from X_{Ma}=0.25 and 0.50. However, it slightly increases to the value of 4.56±0.2 MHz for the glasses with

X_{Ma}=0.75. A various parameters for calculating C_q are shown in Table A4. A larger value of C_q suggests that the perfect cubic symmetry around Al is more deviated, caused by Al-O bond length and bond angle distributions. The topological disorder, referring the degree of deviation from perfect tetrahedral symmetry, decreases with increasing X_{Ma}. The observed trend that the average C_q decreases and then increases with increasing X_{Ma} indicates that the degree of network distortion around Al in $NaAlSiO_4$-$NaBSiO_4$ glasses decreases and then slightly increases with increasing X_{Ma}.

Fig. 8 shows the isotropic projections of the ^{27}Al 3QMAS NMR spectra for $NaAlSiO_4$-$NaBSiO_4$ glasses quenched from melts with varying X_{Ma}. The peak maximum of $^{[4]}$Al in the glasses shifts from -40±1 ppm (X_{Ma}=0) to -38±1 ppm (X_{Ma}=0.25, 0.50, and 0.75). A drastic decrease in the ^{27}Al chemical shift of peak maximum occurs when boron is added into $NaAlSiO_4$ glasses (from X_{Ma}=0 to X_{Ma}=0.25). With increasing X_{Ma} from 0.25 to 0.75, there are no change in the chemical shift of peak maximum. The FWHM for $^{[4]}$Al in the isotropic projections decreases from ~13±1 ppm (X_{Ma}=0) to ~9±1 ppm (X_{Ma}=0.25) and then slightly decreases from ~9±1 ppm (X_{Ma}=0.25) to ~8±1 ppm (X_{Ma}=0.75) (Table A4). These results indicate that the topological disorder in the glasses decreases with increasing X_{Ma}. The $^{[5]}$Al peak (approximately -20 ppm) is resolved in the isotropic projections of the ^{27}Al 3QMAS NMR spectra for $NaAl_{0.25}B_{0.75}SiO_4$ glasses.

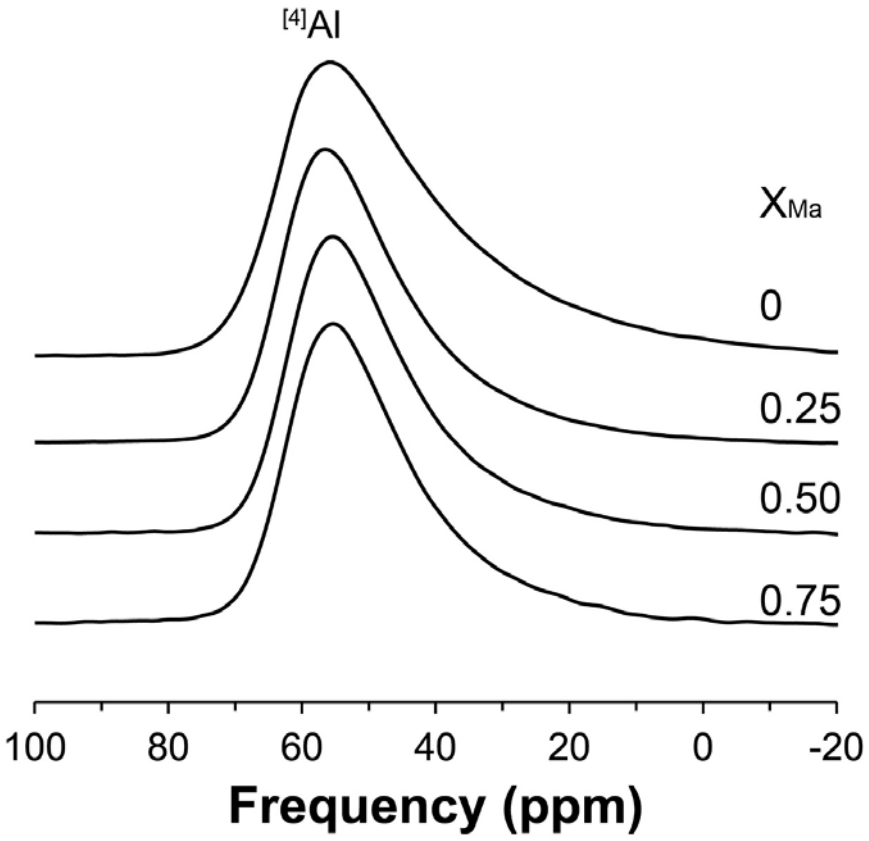

Figure 6. ^{27}Al MAS NMR spectra for $NaAlSiO_4$-$NaBSiO_4$ glasses at 9.4 T with varying X_{Ma}.

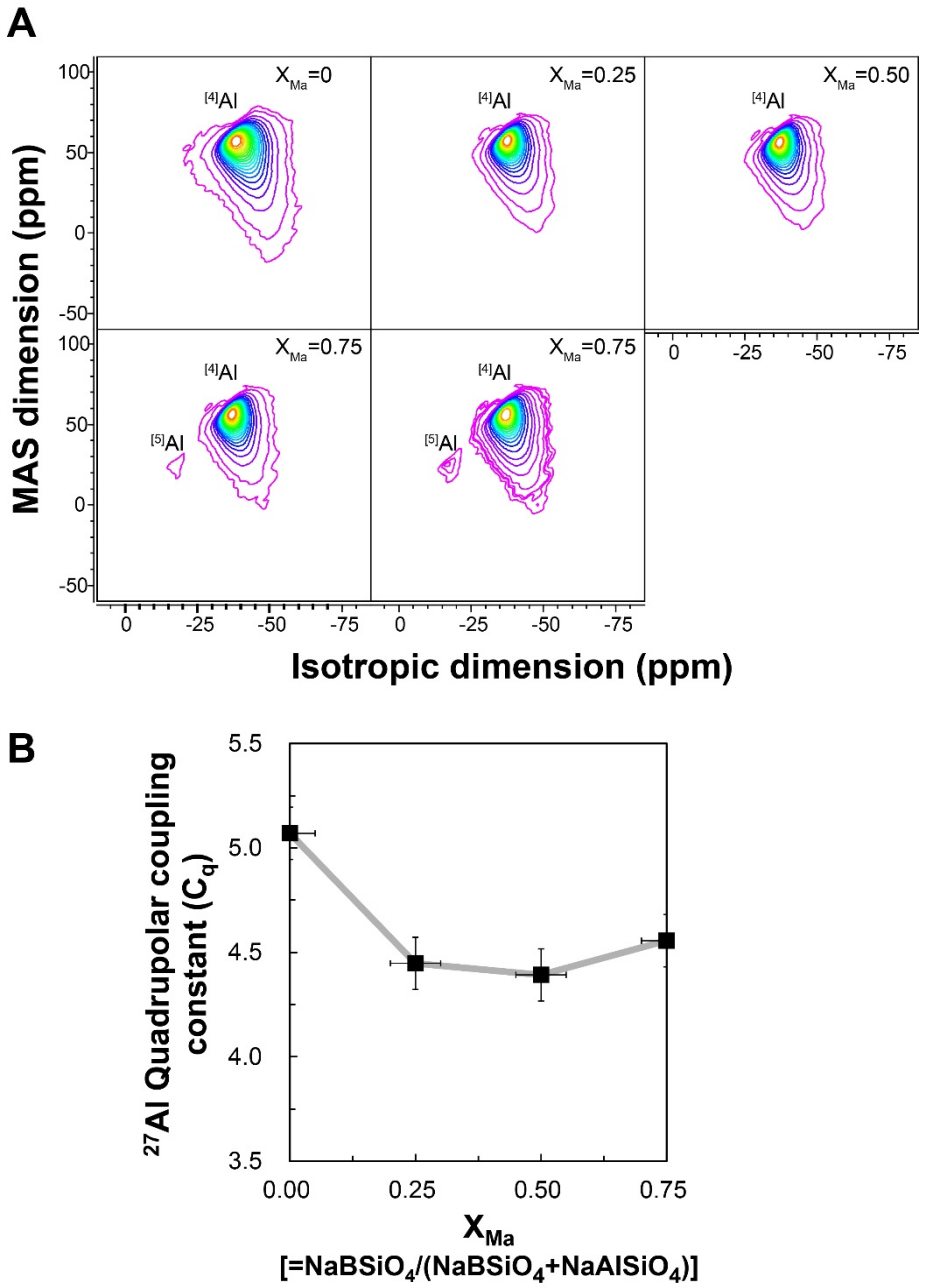

Figure 7. (A) ^{27}Al 3QMAS NMR spectra $NaAlSiO_4$-$NaBSiO_4$ glasses at 9.4 T with varying X_{Ma}. Contour lines are drawn at 5% intervals from relative intensities of 7~92% with added lines at 1%, 2%, and 5% for all the glasses. Contour lines of the last one with X_{Ma}=0.75 are drawn at 6% intervals from relative intensities of 10~88% with added lines at 0.7%, 1.1%, 1.3%, 4%, and 7% to resolve [5]Al. (B) Quadrupolar coupling constant (C_q) of [4]Al in the same glasses with varying X_{Ma}. The asymmetry parameter (η) is assumed to be 0.5.

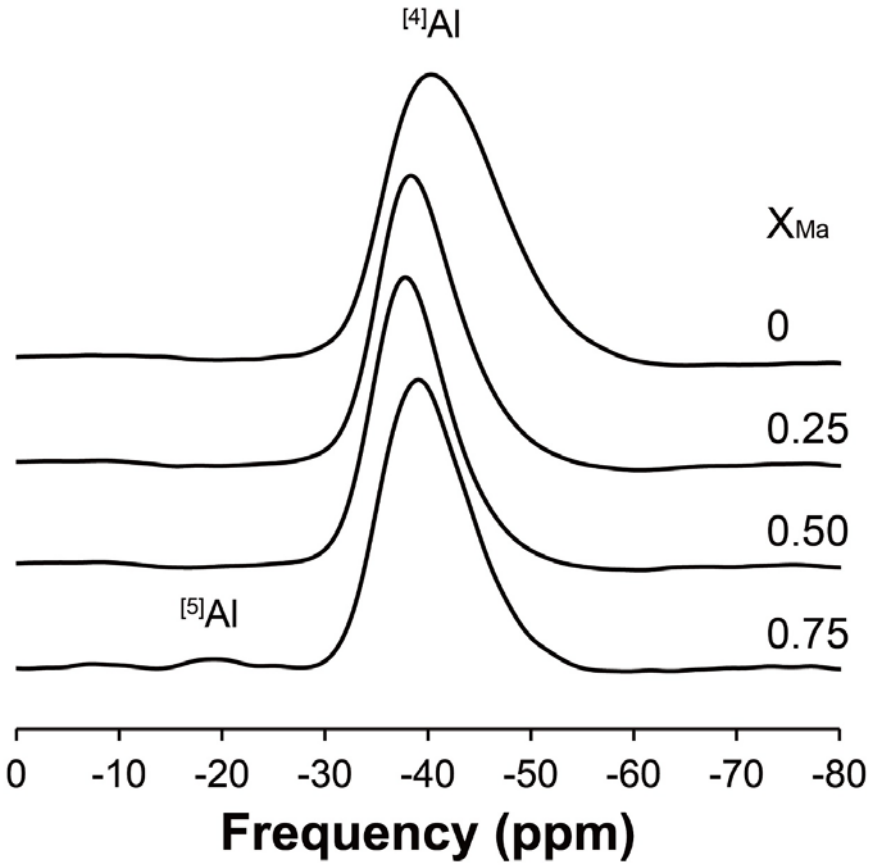

Figure 8. Total isotropic projections of ^{27}Al 3QMAS NMR spectra for $NaAlSiO_4$-$NaBSiO_4$ glasses with varying X_{Ma}.

3.4. Effect of boron fraction [B/(B+Al)] on extent of network connectivity and disorder in boron-bearing nepheline ($NaAlSiO_4$-$NaBSiO_4$) glasses and melts: Insights from ^{17}O MAS and 3QMAS NMR results

Fig. 9 shows the ^{17}O MAS NMR spectra for $NaAlSiO_4$-$NaBSiO_4$ glasses quenched from melts with varying X_{Ma}. For nepheline glasses at X_{Ma}=0, it is well known that there are all BOs ($^{[4]}$Al-O-$^{[4]}$Al, $^{[4]}$Si-O-$^{[4]}$Al, and $^{[4]}$Si-O-$^{[4]}$Si) (Lee and Stebbins, 2000). Therefore, the broad peak between approximately -25~50 ppm in the MAS dimension for nepheline glasses is the sum of the three BOs based on the previous study (Lee and Stebbins, 2000). With increasing X_{Ma}, the broad B-O-B peak between -50~0 ppm in the MAS dimension increases. Note that this assignment is based on the previous study (Lee and Stebbins, 2002). Because the overlap of various peaks in the ^{17}O MAS NMR spectra, the peak assignment and quantification of oxygen network connectivity are difficult. To resolve the peaks, 2D ^{17}O 3QMAS NMR spectra for the glasses are collected. Fig. 10 shows the 2D ^{17}O 3QMAS NMR spectra for $NaAlSiO_4$-$NaBSiO_4$ glasses with varying X_{Ma}. The peaks of BOs ($^{[4]}$Si-O-$^{[4]}$Si, $^{[4]}$Al-O-$^{[4]}$Si) are fully resolved for nepheline glasses with X_{Ma}=0, which is consistent with the previous study (Lee and Stebbins, 2000). The presence of a non-negligible fraction of $^{[4]}$Al-O-$^{[4]}$Al indicates a violation of the Al-avoidance rule in the nepheline glasses due to high Al/Si ratio. The peaks of BOs ($^{[4]}$Si-O-$^{[4]}$Si, B-O-$^{[4]}$Si, and B-O-B) are partially resolved for boron-bearing nepheline glasses in this study. In the spectrum for $NaAl_{0.25}B_{0.75}SiO_4$ glasses (X_{Ma}=0.75), a small but detectable Na-O-B peak is firstly observed in 2D ^{17}O 3QMAS NMR spectra (approximately -25~-45 ppm in the isotropic dimension and approximately 70~90 ppm in the MAS dimension). The peaks of the NBOs (Na-O-$^{[4]}$Si and Na-O-B) are not fully resolved due to overlap with $^{[4]}$Si-O-$^{[4]}$Al peak but can be seen as labeled. With increasing X_{Ma}, the intensities of $^{[4]}$Si-O-$^{[4]}$Si, $^{[4]}$Si-O-B, B-O-B, and Na-O-$^{[4]}$Si increase and those of $^{[4]}$Si-O-$^{[4]}$Al and $^{[4]}$Al-O-$^{[4]}$Al decreases. Note that the peak assignments of BOs and NBOs in the 2D ^{17}O 3QMAS NMR spectra are based on previous studies of boron-bearing silicate glasses (Du and Stebbins, 2003a, b; Lee et al., 2001; Lee and Stebbins, 2002).

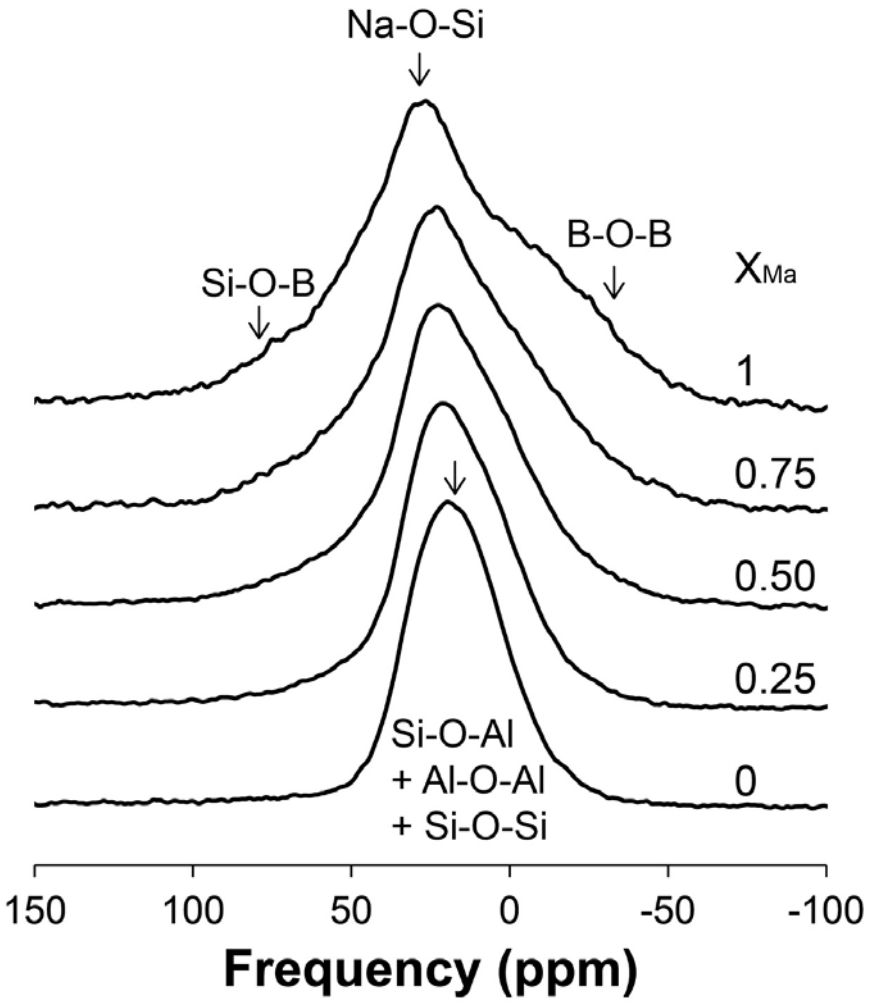

Figure 9. ^{17}O MAS NMR spectra for $NaAlSiO_4$-$NaBSiO_4$ glasses at 9.4 T with varying X_{Ma}.

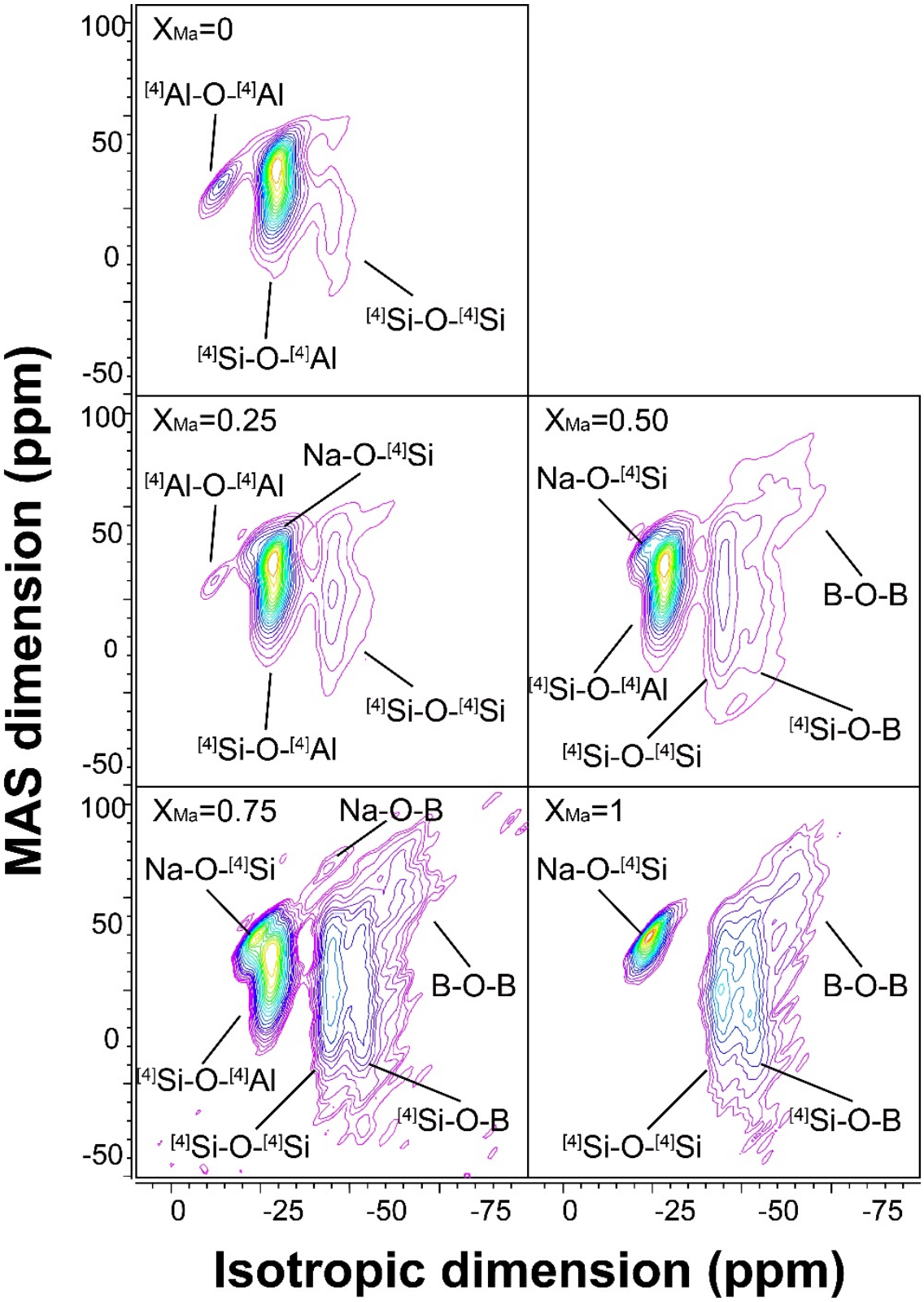
MAS dimension (ppm)
Isotropic dimension (ppm)
XMa=0
[4]Al-O-[4]Al
[4]Si-O-[4]Si
[4]Si-O-[4]Al
XMa=0.25
Na-O-[4]Si
[4]Al-O-[4]Al
[4]Si-O-[4]Si
[4]Si-O-[4]Al
XMa=0.50
Na-O-[4]Si
B-O-B
[4]Si-O-[4]Al
[4]Si-O-B
[4]Si-O-[4]Si
XMa=0.75
Na-O-B
Na-O-[4]Si
B-O-B
[4]Si-O-[4]Al
[4]Si-O-B
[4]Si-O-[4]Si
XMa=1
Na-O-[4]Si
B-O-B
[4]Si-O-B
[4]Si-O-[4]Si
100
50
0
-50
0
-25
-50
-75

Figure 10. ^{17}O 3QMAS NMR spectra for $NaAlSiO_4$-$NaBSiO_4$ glasses at 9.4 T with varying X_{Ma}. Contour lines of the spectra with X_{Ma}=0 are drawn at 5% intervals from relative intensities of 13~88% with added lines at 1%, 3%, 6%, and 9%. Contour lines of the spectra with X_{Ma}=0.25 and 0.50 are drawn at 5% intervals from relative intensities of 13~88% with added lines at 1.5%, 3%, 6%, and 9%. Contour lines of the spectra with X_{Ma}=0.75 are drawn at 5% intervals from relative intensities of 13~93% with added lines at 1.5%, 5%, and 8%. Contour lines of the spectra with X_{Ma}=1 are drawn at 5% intervals from relative intensities of 13~93% with added lines at 3%, 8%, and 8%.

In Fig. 11, the total isotropic projections of the 2D ^{17}O 3QMAS NMR spectra for $NaAlSiO_4$-$NaBSiO_4$ glasses quenched from melts with varying X_{Ma} are shown. A small fraction of $^{[4]}$Al-O-$^{[4]}$Al and $^{[4]}$Si-O-$^{[4]}$Si is resolved for the glasses with X_{Ma}=0 and 0.25. $^{[4]}$Al-O-$^{[4]}$Al and $^{[4]}$Si-O-$^{[4]}$Al decrease (blue letters), and $^{[4]}$Si-O-$^{[4]}$Si, $^{[4]}$Si-O-B, B-O-B, and Na-O-$^{[4]}$Si increase (red letters) with increasing X_{Ma}. In the previous ^{17}O 3QMAS NMR study for B_2O_3-SiO_2 glasses, they assigned the peak between -90~90 ppm in the MAS dimension and -85~-65 ppm in the isotropic dimension as $^{[3]}$B-O-$^{[3]}$B because there exists only $^{[3]}$B from the results of ^{11}B NMR spectra (Lee and Stebbins, 2002). In this study, however, the coordination state of B-O-B peak cannot determined in the ^{17}O 3QMAS NMR spectra because there exist both $^{[3]}$B and $^{[4]}$B from the results of ^{11}B MAS and 3QMAS NMR spectra (Fig. 1A-B). Although the quantitative fraction of BOs and NBOs cannot be determined because the peaks of Na-O-$^{[4]}$Si and $^{[4]}$Si-O-$^{[4]}$Al are overlapped in ^{17}O 2D NMR spectra, a qualitative trend that the NBO (Na-O-$^{[4]}$Si) increases with increasing X_{Ma} can be shown.

The degree of mixing between framework cations, such as B, Al, and Si, can be obtained from ^{17}O NMR spectra for the glasses with varying boron content and can be expressed by the following quasi-chemical equations:

$$^{[4]}\text{Si-O-}^{[4]}\text{Si} + {}^{[4]}\text{Al-O-}^{[4]}\text{Al} \rightarrow 2(^{[4]}\text{Si-O-}^{[4]}\text{Al}) \quad \cdots\cdots (1)$$

$$^{[4]}\text{Si-O-}^{[4]}\text{Si} + \text{B-O-B} \rightarrow 2(^{[4]}\text{Si-O-B}) \quad \cdots\cdots (2)$$

$$^{[4]}\text{Al-O-}^{[4]}\text{Al} + \text{B-O-B} \rightarrow 2(^{[4]}\text{Al-O-B}) \quad \cdots\cdots (3)$$

The equilibrium constant (K) can be calculated from each quasi-chemical equations, where K_i refers the equilibrium constant of equation i, i=1, 2, 3, based on ^{17}O NMR results. For nepheline glasses, it can be estimated that K_1 is larger than 1 indicating that the formation of $^{[4]}$Si-O-$^{[4]}$Al is favored. When Al and B are both present in the silicate glasses, K_1 and K_3 decrease while K_2 increases with increasing B/(B+Al). The value of K_3 less than 1 means that the mixing between Al and B is not favored. For malinkoite glasses, K_2 is larger than 1, indicating the degree of mixing between Si and B increases with increasing boron content.

In $NaAlSiO_4$-$NaBSiO_4$ glasses, only Na can play a role as a network modifying cation. It is well known that Na-O-Al is not favored in sodiumaluminosilicate glasses

because Na exists for charge-balancing cation for tetrahedral Al. There are two candidates of Na-NBO : Na-O-B, and Na-O-Si. The preference of NBOs in glasses can be expressed:

$$^{[4]}\text{Si-O-B} + \text{Na-O-B} \rightarrow \text{B-O-B} + \text{Na-O-}^{[4]}\text{Si} \quad \cdots\cdots (1)$$

$$^{[4]}\text{Si-O-}^{[4]}\text{Si} + \text{Na-O-B} \rightarrow {}^{[4]}\text{Si-O-B} + \text{Na-O-}^{[4]}\text{Si} \quad \cdots\cdots (2)$$

Although a small amount of Na-O-B is detected in $NaAl_{0.25}B_{0.75}SiO_4$ glasses (X_{Ma}=0.75), Na-O-Si is evidently favored than Na-O-B. Because the formation of $^{[4]}$Si-O-B is preferred to the formation of B-O-B and $^{[4]}$Si-O-$^{[4]}$Si with increasing boron content, quasi-chemical reaction (2) is favored than reaction (1).

The ^{17}O NMR results can also help constrain the role of non-framework cation in the glasses. In this study, it is observed that the Na-O-Si peak (~-20 ppm in isotropic dimension, see Fig. 11) increases with increasing B/(B+Al). From the fact that the ratio Na/(B+Al) is the same in all glasses, an increase in the Na-O-Si peak indicates that the role of Na changes. The change in role of non-framework cation in glasses can be described using the following quasi-chemical equations, (1), (2), (3) for nepheline glasses, (4) for $NaAl_{0.5}B_{0.5}SiO_4$ glasses, and (5) for malinkoite glasses, where asterisk (*) refers charge-balancing cations:

$$2(\text{Na-O-}^{[4]}\text{Si}) \rightarrow 2\text{Na}^* \text{ --- } ^{[4]}\text{Si-O-}^{[4]}\text{Si} \quad \cdots\cdots (1)$$

$$2(\text{Na-O-}^{[4]}\text{Al}) \rightarrow 2\text{Na}^* \text{ --- } ^{[4]}\text{Al-O-}^{[4]}\text{Al} \quad \cdots\cdots (2)$$

$$\text{Na-O-}^{[4]}\text{Si} + \text{Na-O-}^{[4]}\text{Al} \rightarrow 2\text{Na}^* \text{ --- } ^{[4]}\text{Si-O-}^{[4]}\text{Al} \quad \cdots\cdots (3)$$

$$^{[4]}\text{Si-O-}^{[4]}\text{Si} + {}^{[3,4]}\text{B-O-}^{[3,4]}\text{B} + \text{Na}^* \rightarrow {}^{[4]}\text{Si-O-}^{[4]}\text{B-O-}^{[3]}\text{B} + \text{Na-O-}^{[4]}\text{Si} \quad \cdots\cdots (4)$$

$$^{[4]}\text{Si-O-}^{[4]}\text{Si} \text{ --- } 2\text{Na}^* \rightarrow 2(\text{Na-O-}^{[4]}\text{Si}) \quad \cdots\cdots (5)$$

For nepheline glasses, the current results indicate that the formation of three BOs, $^{[4]}$Si-O-$^{[4]}$Si, $^{[4]}$Si-O-$^{[4]}$Al, and $^{[4]}$Al-O-$^{[4]}$Al is favored. Thus, Na play a role as charge-balancing cation (Na*). When there exist both B and Al in $NaAl_{0.5}B_{0.5}SiO_4$ glasses, Na plays a dual role as a charge-balancing cation (Na*) and network modifying cation. For malinkoite glasses, the formation of Na-O-$^{[4]}$Si is favored, indicating that Na play a role as network modifying cation. It is noted that because there is no detectable Na-O-B peak, the formation of Na-O-B is not considered in quasi-chemical equations for $NaAl_{0.5}B_{0.5}SiO_4$ and malinkoite glasses.

These results show that the role of Na changes from charge-balancing cation (for nepheline glasses) to network-modifying cations forming NBO (for malinkoite glasses).

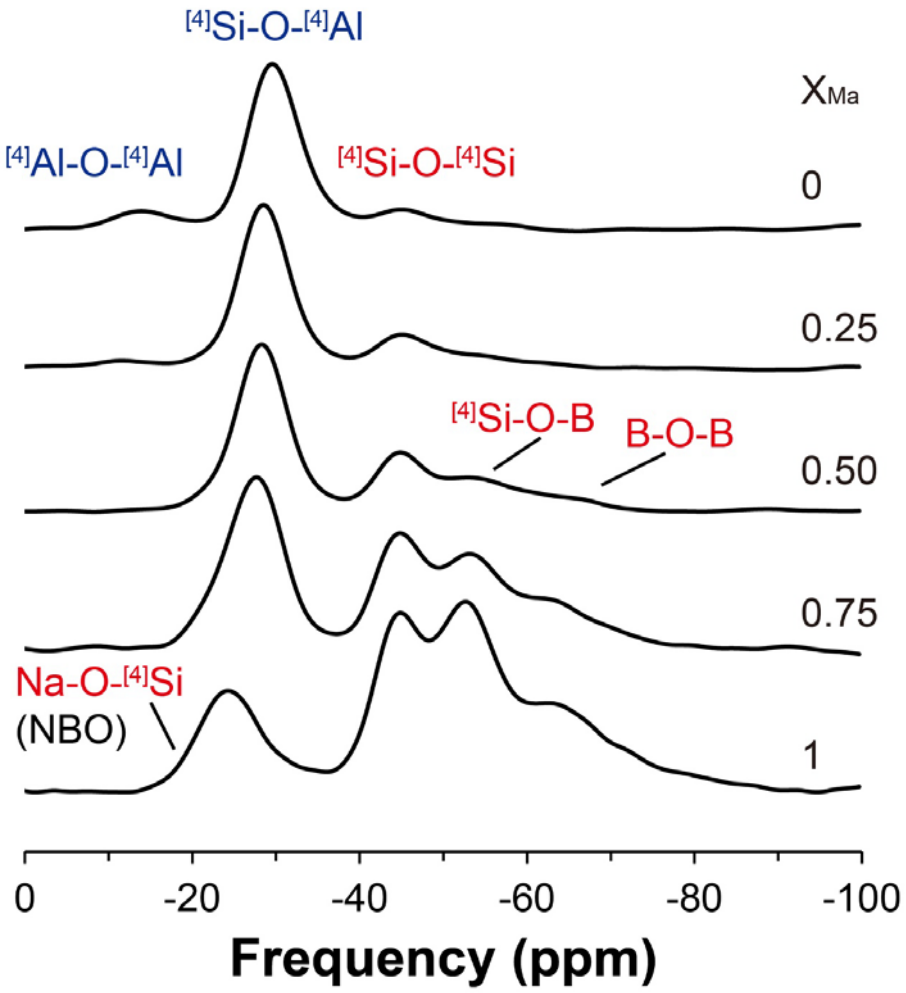

Figure 11. Total isotropic projections of ^{17}O 3QMAS NMR spectra for $NaAlSiO_4$-$NaBSiO_4$ glasses with varying X_{Ma}.

3.5. Effect of boron content on B coordination environments in boron-bearing albite ($NaAlSi_3O_8$-$NaBSi_3O_8$) glasses and melts: Insights from ^{11}B MAS and 3QMAS NMR results

Fig. 12 shows ^{11}B MAS NMR spectra for $NaAlSi_3O_8$-$NaBSi_3O_8$ glasses quenched from melts with varying X_{Rd} [=$NaBSi_3O_8$/($NaBSi_3O_8$+$NaAlSi_3O_8$)]. The ratio of Na/B+Na is 0.8 (X_{Rd}=0.25), 0.67 (X_{Rd}=0.50), 0.57 (X_{Rd}=0.75), and 0.5 (X_{Rd}=1) for each glass. Since there are no ring ($^{[3]}B$) species above X_{Na}=0.33 in Na_2O-B_2O_3 glasses in this study, it is assumed to be only non-ring ($^{[3]}B$) in boron-bearing albite glasses. As X_{Rd} increases from 0.25 to 1, $^{[4]}B$ increases and non-ring ($^{[3]}B$) decreases. Two boron coordination-environments are partially resolved in the ^{11}B MAS NMR spectra.

Because it is assumed that there are only non-ring ($^{[3]}B$) species in $NaAlSi_3O_8$-$NaBSi_3O_8$ glasses, the simulation was performed with $^{[4]}B$ and non-ring ($^{[3]}B$) species using the software Dmfit with *Q MAS 1/2* function. The population of boron species of boron-bearing albite glasses is shown in Fig. 13. Non-ring ($^{[3]}B$) decreases from ~30% to ~10% and $^{[4]}B$ increases from ~70% to ~90% as X_{Rd} increases. The simulation results are shown in Appendix A2. The previous study reported that there are 60% and 30% of non-ring ($^{[3]}B$) in $NaAl_{0.8}B_{0.2}Si_3O_8$ and $NaBSi_3O_8$ glasses, respectively (Geisinger et al., 1988). The uncertainty can arise from the fitting method (NMRCAP) and the background subtraction of ^{11}B MAS NMR spectra they collected at 11.7 T although magnetic field is stronger than 9.4 T in this study. Since $^{[3]}B$ and $^{[4]}B$ are not fully resolved at 11.7 T in the same manner at 9.4 T, the uncertainty of fitting two peaks could be caused.

Fig. 14 shows ^{11}B MAS NMR spectra for $NaAlSiO_4$-$NaBSiO_4$ (black lines) and $NaAlSi_3O_8$-$NaBSi_3O_8$ (red lines) glasses with B/(B+Al)=0.25 and 1. Comparing boron environments with different B/Si ratio and same B/(B+Al) ratio, the ^{11}B chemical shift decreases toward negative frequency with increasing B/Si ratio (from boron-bearing nepheline glasses to albite glasses) in Fig. 14. Since the spectra were normalized to $^{[4]}B$ peak, the fraction of non-ring ($^{[3]}B$) is smaller in high B/Si ratio. Fig. 15 shows the population of B species for two amorphous system in this study. There are more $^{[4]}B$ in albite-reedmergnerite glasses than in nepheline-malinkoite glasses.

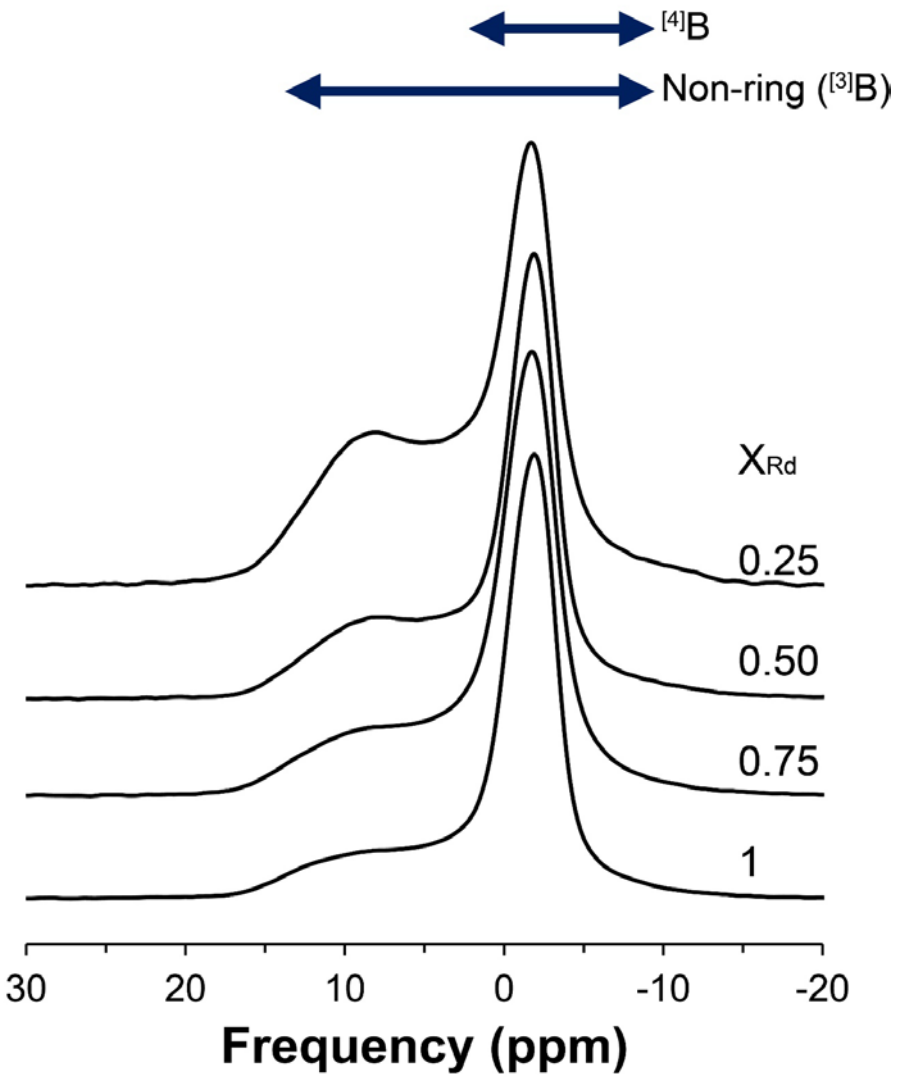

Figure 12. ^{11}B MAS NMR spectra for $NaAlSi_3O_8$-$NaBSi_3O_8$ glasses at 9.4 T with varying mole fraction of reedmergnerite component [X_{Rd}=$NaBSi_3O_8$/($NaBSi_3O_8$+$NaAlSi_3O_8$)].

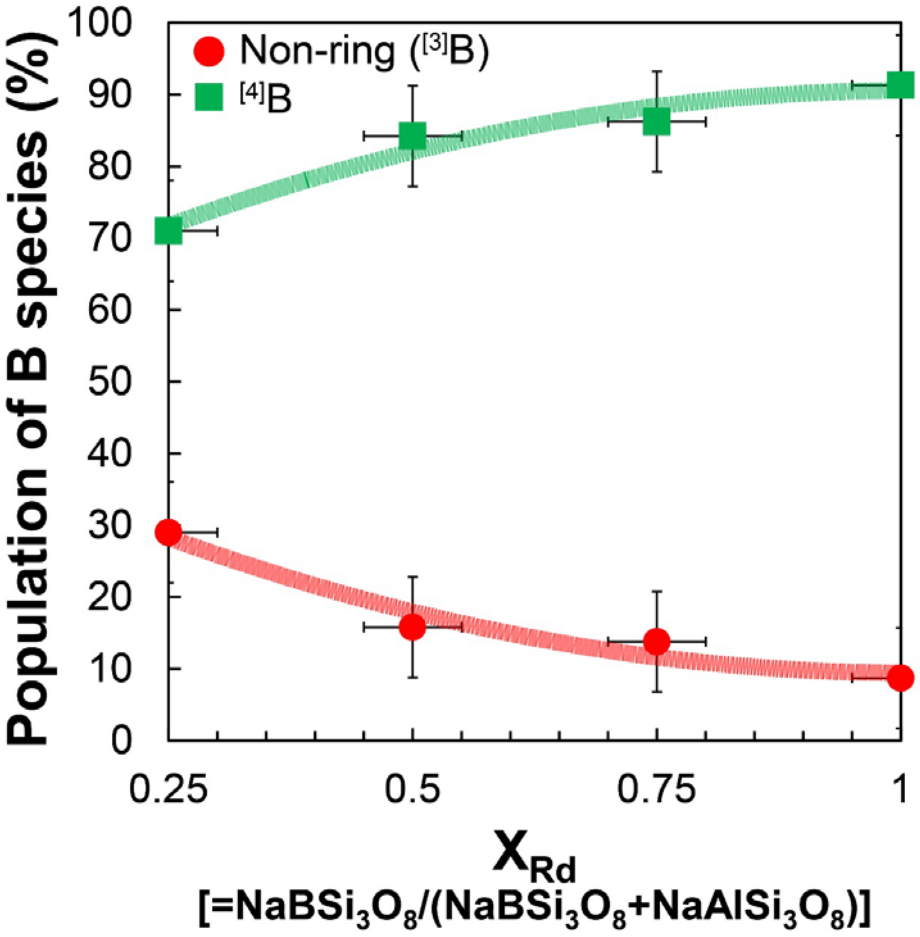

Figure 13. The population of boron species from ^{11}B MAS NMR spectra for $NaAlSi_3O_8$-$NaBSi_3O_8$ glasses with varying X_{Rd}. The blue and red circles refer to the population of ring ($^{[3]}$B) and non-ring ($^{[3]}$B), respectively. The green square refers to the population of $^{[4]}$B. Error bar was estimated from the uncertainty in sample composition, phasing of NMR spectrum, and NMR processing conditions.

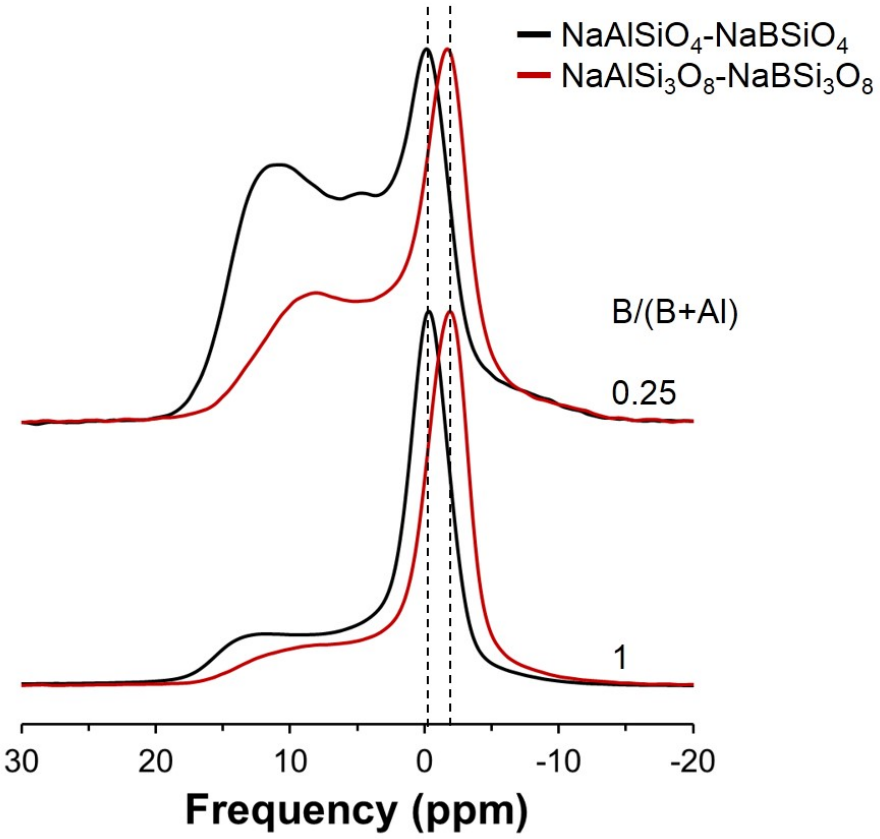

Figure 14. ^{11}B MAS NMR spectra for $NaAlSiO_4$-$NaBSiO_4$ (black) and $NaAlSi_3O_8$-$NaBSi_3O_8$ (red) glasses at 9.4 T with the same B/(B+Al) ratio, 0.25 and 1.

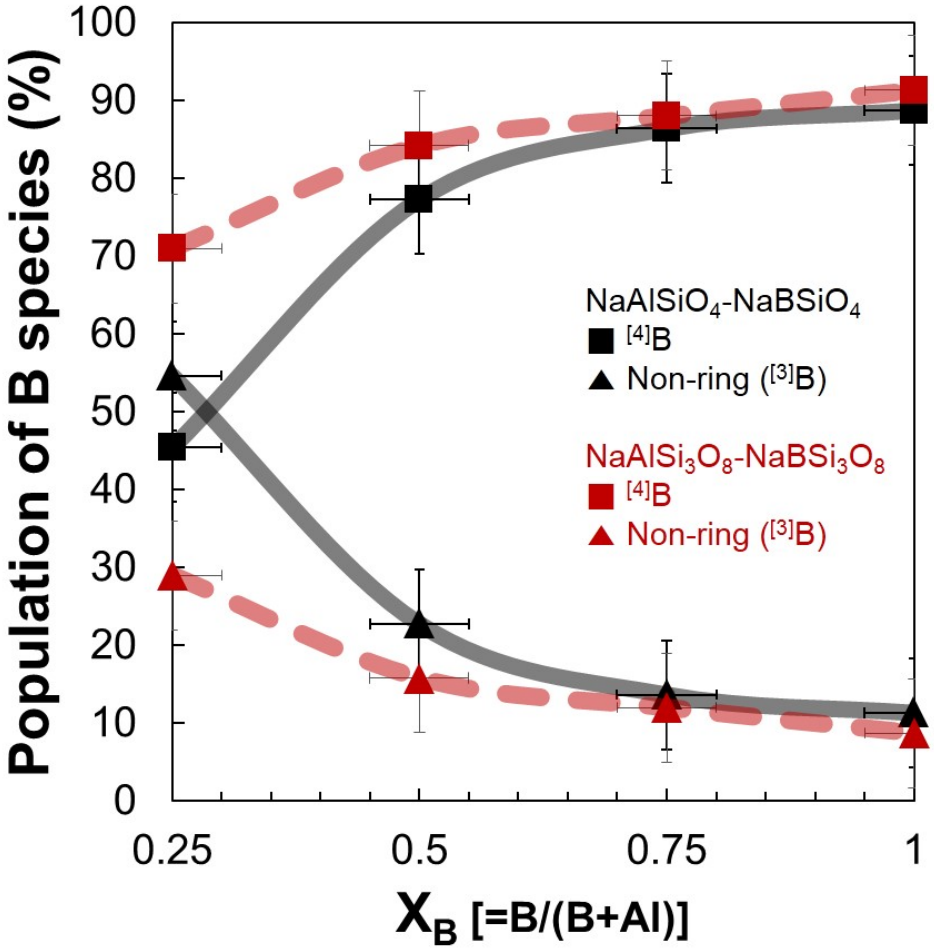

Figure 15. The population of boron species from ^{11}B MAS NMR spectra for $NaAlSiO_4$-$NaBSiO_4$ (black) and $NaAlSi_3O_8$-$NaBSi_3O_8$ (red) glasses with varying B/(B+Al) ratio.

4. DISCUSSION

4.1. New interpretation of ^{11}B NMR spectra for boron-bearing glasses containing non-framework cation based on quantum chemical calculations

A lot of ^{11}B NMR studies have followed the peak assignment of topological species of $^{[3]}B$ based on the previous B_2O_3-SiO_2 NMR study (Lee and Stebbins, 2002). However, since B and Si are both network forming cations, there is a possibility of a different interpretation of ^{11}B NMR spectra for boron-bearing glasses containing non-framework cations. The current study suggests that the peak position of non-ring ($^{[3]}B$) can be changed with varying sodium content based on quantum chemical calculations (see Appendix A1 for more details). Fig. 1C shows the total isotropic projections of ^{11}B 3QMAS NMR spectra and the simulation results for the glasses with X_{Na}=0 and 0.14 to resolve ring and non-ring ($^{[3]}B$) peaks. The bold black thick line refers experimental data for total isotropic projections experimental. The thin black, blue, red, and green lines refer total simulation, ring ($^{[3]}B$), non-ring ($^{[3]}B$), and $^{[4]}B$. With increasing X_{Na} from 0 to 0.14, the NMR chemical shift of non-ring ($^{[3]}B$) increases from ~42.5 ppm to ~46 ppm in the isotropic dimension, the fraction of ring ($^{[3]}B$) decreases from ~78% to ~70%, and the fraction of non-ring ($^{[3]}B$) does not change with the value of ~22%, and the fraction of $^{[4]}B$ increases from 0% to ~8%. The change in ^{11}B NMR chemical shift in isotropic dimension of non-ring ($^{[3]}B$) is approximately 3.5 ppm. This interpretation is more plausible considering that ring ($^{[3]}B$) is more stable than non-ring ($^{[3]}B$). Thus, ring ($^{[3]}B$) is consumed to form $^{[4]}B$ before non-ring ($^{[3]}B$) converts to $^{[4]}B$. From these results, this study propose that the peak assignment of ^{11}B NMR spectra should be carefully done for the glasses with non-framework cations.

4.2. Insights into dissolution rate and viscosity of boron-bearing sodium aluminosilicate melts based on boron environment and oxygen network connectivity

The previous study of the change in dissolution rate of $NaAlSiO_4$-$NaBSiO_4$ glasses suggested that a drastic increase of dissolution rate with boron content is due to a significant drop of non-ring ($^{[3]}B$) species (Pierce et al., 2010). There could be some uncertainties of their simulation results because of following reasons. First, because they assigned the topological species of $^{[3]}B$ based on borosilicate glasses even though the system in their study has non-

framework cation, the population of ring ($^{[3]}$B) species can be overestimated. Second, the fitting function they used, Gaussian, is not proper function when fitting quadurpolar nuclear like boron. These uncertainties may lead an inappropriate explanation of mechanism of dissolution rate. Since the change in atomic structure around boron seems not to explain the change in dissolution rate with varying boron content in this study, the new mechanism of dissolution rate is required not based on atomic structure of boron but based on oxygen network connectivity.

An increase in Na-O-$^{[4]}$Si implies that the role of sodium changes from charge-balancing cation to network modifying cation, forming NBO. When sodium forms Na-O-$^{[4]}$Si, boron bonds with $^{[4]}$Si and the coordination state is four. B-O-B and B-O-$^{[4]}$Si are relatively weak BOs, thus, it is understandable that the dissolution rate increases with increasing B-O-B and B-O-$^{[4]}$Si fraction. A decrease in viscosity can be also explained by an increase in Na-O-$^{[4]}$Si. The schematic diagram of the atomic configuration of $NaAlSiO_4$-$NaBSiO_4$ glasses with varying Al/B ratio is shown in Fig. 16. Fig. 16A shows that there are no NBOs and Na plays a charge-balancing cation in $NaAlSiO_4$ glasses. Si and Al are both four-coordinated. When Al and B both exist, Na forms Na-O-$^{[4]}$Si (yellow shadow) indicating that Na plays a dual role as charge-balancing and network modifying cation, and $^{[3]}$B converts into $^{[4]}$B bonding with $^{[4]}$Si in $NaAl_{0.5}B_{0.5}SiO_4$ glasses in Fig. 16B. For $NaBSiO_4$ glasses, the connection between boron increases, and all Na play a role as a network-modifying cation forming Na-O-$^{[4]}$Si in Fig. 16C.

The dissolution of element occurs along weak bond. If there are abundant Na-O-B, it could be predicted that the drastic increase of dissolution rate of boron is due to the breakage of Na-O-B. However, in this study, ^{17}O 3QMAS NMR spectra for $NaAlSiO_4$-$NaBSiO_4$ glasses with varying X_{Ma} do not show an abundant Na-O-B implying that there are other factors to affect the dissolution rate rather than the breakage of NBO. It is observed that B-O-B and B-O-$^{[4]}$Si increase with increasing boron content. Because B-O-B and B-O-$^{[4]}$Si are considered weaker than other BOs, the dissolution of boron occurs along breaking B-O-B and B-O-$^{[4]}$Si. Therefore, this study propose that the origin of the change in dissolution rate of boron in boron-bearing aluminosilicate melts and glasses is not attributed to the change in boron environment but to the change in oxygen network connectivity, especially B-O-B and B-O-$^{[4]}$Si.

It is well established that the viscosity is proportional to $\exp[A/(B+X_{NBO})]$, where A and B are constant, and X_{NBO} is the fraction of NBOs (Giordano and Dingwell, 2003a; Lee et al., 2004). From the oxygen connectivity, the change in viscosity of boron-bearing granitic and pegmatitic melts can be explained by the fraction of NBO (Na-O-$^{[4]}$Si), indicating the degree of polymerization of silicate melts. Although there are no available viscosity measurements of melts and glasses which have the same composition with the glasses in this study, the tendency of an increase in Na-O-$^{[4]}$Si can be estimated assuming the constant B/Si and B/Na ratio. The composition of boron-bearing granitic melts and glasses is closer to boron-bearing albite glasses. Therefore, the detailed information on oxygen network connectivity of boron-bearing albite glasses is required to explain the change in viscosity (Lee and Lee, in preparation).

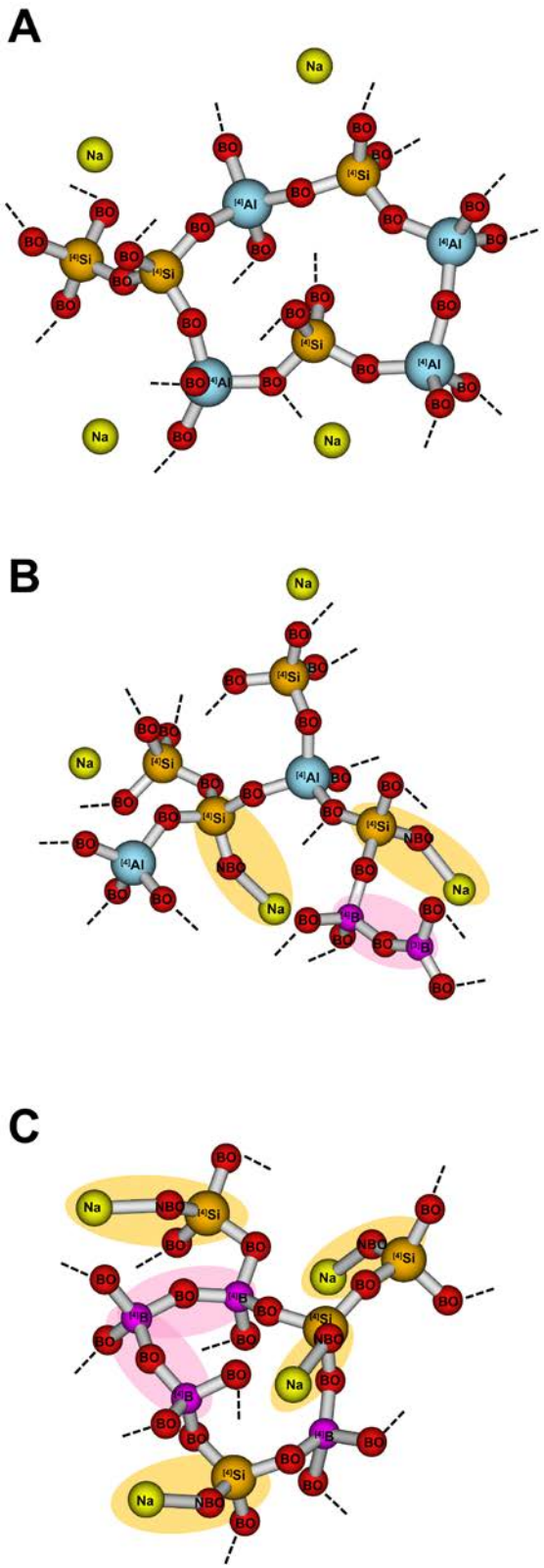

Figure 16. The schematic diagram of the atomic configuration of $NaAlSiO_4$-$NaBSiO_4$ glasses with varying B/(B+Al) ratio.

5. CONCLUSION

The results from the quantum chemical calculations presented in this study imply that ^{11}B NMR chemical shift can increase with increasing sodium content in boron-bearing glasses containing non-framework cation like Na. In contrast with the previous interpretation that non-ring ($^{[3]}B$) decreases with increasing sodium content, the current study determines that non-ring ($^{[3]}B$) does not change with varying sodium content. The experimental data presented here provide structural details of atomic configurations around B and Al, their connectivity (through changes in NBO and BO environments), and the extent of chemical and topological disorder in multicomponent boron-bearing silicate glasses in the nepheline-malinkoite and albite-reedmergnerite pseudobinary join. The ^{11}B MAS and 3QMAS NMR spectra for all the multicomponent silicate glasses show $^{[4]}B$ increases at the expense of non-ring ($^{[3]}B$) with increasing boron content, assuming that ring ($^{[3]}B$) does not exist due to high Na/B ratio. The quantification of boron environment from ^{11}B MAS NMR spectra show that there are more $^{[4]}B$ in albite-reedmergnerite glasses than in nepheline-malinkoite glasses. The ^{27}Al MAS and 3QMAS NMR spectra for $NaAlSiO_4$-$NaBSiO_4$ glasses show a dominant $^{[4]}Al$. With high boron content (X_{Ma}=0.75), a small but detectable amount of $^{[5]}Al$ is observed. The spectral analysis of $^{[4]}Al$ peak suggests that the degree of distortion around Al coordination decreases with the addition of boron into nepheline glasses. The ^{17}O 3QMAS NMR spectra for $NaAlSiO_4$-$NaBSiO_4$ glasses show that Na-O-$^{[4]}Si$, B-O-B, and B-O-$^{[4]}Si$ increase with increasing X_{Ma}.

The relationship between the dissolution rate and oxygen network connectivity is proposed in this study based on ^{17}O 3QMAS NMR spectra for $NaAlSiO_4$-$NaBSiO_4$ glasses. The dissolution of boron from the glasses occurs by breaking the relatively weak BOs (B-O-B and B-O-$^{[4]}Si$) not by changing the boron environment suggested by the previous study. An increase in NBO fraction can also explain the drop of viscosity of boron-bearing granitic melts. The composition of boron-bearing granitic melts and glasses is closer to boron-bearing albite glasses. Therefore, the detailed information on oxygen network connectivity of boron-bearing albite glasses is required to explain the change in viscosity (Lee and Lee, in preparation).

References

Bartels, A., Behrens, H., Holtz, F., Schmidt, B.C., Fechtelkord, M., Knipping, J., Crede, L., Baasner, A. and Pukallus, N. (2013) The effect of fluorine, boron and phosphorus on the viscosity of pegmatite forming melts. *Chemical Geology* **346**, 184-198.

Becke, A.D. (1993) A new mixing of Hartree–Fock and local density-functional theories. *The Journal of Chemical Physics* **98**, 1372-1377.

Bray, P.J. (1985a) Nuclear magnetic resonance studies of glass structure. *Journal of Non-Crystalline Solids* **73**, 19-45.

Bray, P.J. (1985b) Nuclear magnetic resonance studies of glass structure. *Journal of Non-Crystalline Solids* **73**, 19-45.

Dhara, A., Mishra, R.K., Shukla, R., Valsala, T.P., Sudarsan, V., Tyagi, A.K. and Kaushik, C.P. (2016) A comparative study on the structural aspects of sodium borosilicate glasses and barium borosilicate glasses: Effect of Al2O3 addition. *Journal of Non-Crystalline Solids* **447**, 283-289.

Dingwell, D., Knoche, R., Webb, S. and Pichavant, M. (1992) The effect of B_2O_3 on the viscosity of haplogranitic liquids. *American Mineralogist* **77**, 457-461.

Du, L.-S. and Stebbins, J.F. (2003a) Nature of silicon-boron mixing in sodium borosilicate glasses: a high-resolution ^{11}B and ^{17}O NMR study. *The Journal of Physical Chemistry B* **107**, 10063-10076.

Du, L.-S. and Stebbins, J.F. (2003b) Site preference and Si/B mixing in mixed-alkali borosilicate glasses: a high-resolution ^{11}B and ^{17}O NMR study. *Chemistry of materials* **15**, 3913-3921.

Du, L.-S. and Stebbins, J.F. (2003c) Solid-state NMR study of metastable immiscibility in alkali borosilicate glasses. *Journal of Non-Crystalline Solids* **315**, 239-255.

Ferlat, G., Charpentier, T., Seitsonen, A.P., Takada, A., Lazzeri, M., Cormier, L., Calas, G. and Mauri, F. (2008) Boroxol rings in liquid and vitreous B_2O_3 from first principles. *Physical Review Letters* **101**, 065504.

Frisch, M., Trucks, G., Schlegel, H., Scuseria, G., Robb, M., Cheeseman, J., Montgomery Jr, J., Vreven, T., Kudin, K. and Burant, J. (2004) Gaussian 03. Gaussian. *Inc.: Wallingford, CT*.

Geisinger, K.L., Oestrike, R., Navrotsky, A., Turner, G.L. and Kirkpatrick, R.J. (1988)

Thermochemistry and structure of glasses along the join $NaAlSi_3O_8$-$NaBSi_3O_8$. *Geochimica Et Cosmochimica Acta* **52**, 2405-2414.

Gin, S., Ryan, J.V., Schreiber, D.K., Neeway, J. and Cabie, M. (2013) Contribution of atom-probe tomography to a better understanding of glass alteration mechanisms: Application to a nuclear glass specimen altered 25 years in a granitic environment. *Chemical Geology* **349**, 99-109.

Giordano, D. and Dingwell, D.B. (2003a) Non-Arrhenian multicomponent melt viscosity: a model. *Earth and Planetary Science Letters* **208**, 337-349.

Giordano, D. and Dingwell, D.B. (2003b) Non-Arrhenian multicomponent melt viscosity: a model. *Earth and Planetary Science Letters* **208**, 337-349.

Hopf, J., Kerisit, S.N., Angeli, F., Charpentier, T., Icenhower, J.P., McGrail, B.P., Windisch, C.F., Burton, S.D. and Pierce, E.M. (2016a) Glass-water interaction: Effect of high-valence cations on glass structure and chemical durability. *Geochimica Et Cosmochimica Acta* **181**, 54-71.

Hopf, J., Kerisit, S.N., Angeli, F., Charpentier, T., Icenhower, J.P., McGrail, B.P., Windisch, C.F., Burton, S.D. and Pierce, E.M. (2016b) Glass–water interaction: Effect of high-valence cations on glass structure and chemical durability. *Geochimica et cosmochimica Acta* **181**, 54-71.

Hwang, S.J., Fernandez, C., Amoureux, J.P., Cho, J., Martin, S.W. and Pruski, M. (1997) Quantitative study of the short range order in B_2O_3 and B_2S_3 by MAS and two-dimensional triple-quantum MAS ^{11}B NMR. *Solid State Nuclear Magnetic Resonance* **8**, 109-121.

Kilymis, D., Delaye, J.-M. and Ispas, S. (2016) Nanoindentation of the pristine and irradiated forms of a sodium borosilicate glass: insights from molecular dynamics simulations. *The Journal of Chemical Physics* **145**, 044505.

Kriz, H.M. and Bray, P.J. (1971) A study of the distribution of boron sites in glassy B_2O_3 using ^{11}B NMR. *Journal of Non-Crystalline Solids* **6**, 27-36.

Lee, A.C. and Lee, S.K. (2016) Effect of boron content on atomic structure of boron-bearing multicomponent oxide glasses: a view from solid-state NMR. *Journal of the mineralogical society of Korea* **29**, 155-165.

Lee, S.K. (2005) Microscopic origins of macroscopic properties of silicate melts and glasses at ambient and high pressure: Implications for melt generation and dynamics. *Geochimica Et Cosmochimica Acta* **69**, 3695-3710.

Lee, S.K., Cody, G.D., Fei, Y. and Mysen, B.O. (2004) Nature of polymerization and properties of silicate melts and glasses at high pressure. *Geochimica Et Cosmochimica Acta* **68**, 4189-4200.

Lee, S.K., Eng, P.J., Mao, H.-K., Meng, Y., Newville, M., Hu, M.Y. and Shu, J. (2005a) Probing of bonding changes in B_2O_3 glasses at high pressure with inelastic X-ray scattering. *Nature Materials* **4**, 851-854.

Lee, S.K., Eng, P.J., Mao, H.-k., Meng, Y. and Shu, J. (2007) Structure of alkali borate glasses at high pressure: B and Li K-edge inelastic X-ray scattering study. *Physical Review Letters* **98**, 105502.

Lee, S.K., Mibe, K., Fei, Y., Cody, G.D. and Mysen, B.O. (2005b) Structure of B_2O_3 glass at high pressure: a B-11 solid-state NMR study. *Physical Review Letters* **94**, 165507.

Lee, S.K., Musgrave, C.B., Zhao, P. and Stebbins, J.F. (2001) Topological disorder and reactivity of borosilicate glasses: quantum chemical calculations and ^{17}O and ^{11}B NMR study. *The Journal of Physical Chemistry B* **105**, 12583-12595.

Lee, S.K. and Stebbins, J.F. (2000) Al–O–Al and Si–O–Si sites in framework aluminosilicate glasses with Si/Al=1: quantification of framework disorder. *Journal of Non-Crystalline Solids* **270**, 260-264.

Lee, S.K. and Stebbins, J.F. (2002) Extent of intermixing among framework units in silicate glasses and melts. *Geochimica Et Cosmochimica Acta* **66**, 303-309.

Lodders, K. and Fegley, B. (1998) The Planetary Science Companion. Oxford Univ. Press, New York.

Lyubetskaya, T. and Korenaga, J. (2007) Chemical composition of Earth's primitive mantle and its variance: 1. Method and results. *Journal of Geophysical Research: Solid Earth* **112**.

Massiot, D., Fayon, F., Capron, M., King, I., Le Calvé, S., Alonso, B., Durand, J.O., Bujoli, B., Gan, Z. and Hoatson, G. (2002) Modelling one-and two-dimensional solid-state NMR spectra. *Magnetic Resonance in Chemistry* **40**, 70-76.

McCloy, J., Washton, N., Gassman, P., Marcial, J., Weaver, J. and Kukkadapu, R. (2015) Nepheline crystallization in boron-rich alumino-silicate glasses as investigated by multi-nuclear NMR, Raman, & Mossbauer spectroscopies. *Journal of Non-Crystalline Solids* **409**, 149-165.

Nicoleau, E., Schuller, S., Angeli, F., Charpentier, T., Jollivet, P., Le Gac, A., Fournier, M., Mesbah, A. and Vasconcelos, F. (2015) Phase separation and crystallization effects on the structure and

durability of molybdenum borosilicate glass. *Journal of Non-Crystalline Solids* **427**, 120-133.

Palme, H. and O'Neill, H.S.C. (2003) Cosmochemical estimates of mantle composition. *Treatise on geochemistry* **2**, 1-38.

Park, S.Y. and Lee, S.K. (2012) Structure and disorder in basaltic glasses and melts: Insights from high-resolution solid-state NMR study of glasses in diopside-Ca-tschermakite join and diopside-anorthite eutectic composition. *Geochimica et cosmochimica Acta* **80**, 125-142.

Park, S.Y. and Lee, S.K. (2014) High-resolution solid-state NMR study of the effect of composition on network connectivity and structural disorder in multi-component glasses in the diopside and jadeite join: implications for structure of andesitic melts. *Geochimica Et Cosmochimica Acta* **147**, 26-42.

Pierce, E.M., Reed, L.R., Shaw, W.J., McGrail, B.P., Icenhower, J.P., Windisch, C.F., Cordova, E.A. and Broady, J. (2010) Experimental determination of the effect of the ratio of B/Al on glass dissolution along the nepheline (NaAlSiO4)-malinkoite (NaBSiO4) join. *Geochimica Et Cosmochimica Acta* **74**, 2634-2654.

Rajmohan, N., Frugier, P. and Gin, S. (2010) Composition effects on synthetic glass alteration mechanisms: Part 1. Experiments. *Chemical Geology* **279**, 106-119.

Rudnick, R.L. and Gao, S. (2003) 3.01 - Composition of the Continental Crust A2 - Holland, Heinrich D, in: Turekian, K.K. (Ed.), Treatise on geochemistry. Pergamon, Oxford, pp. 1-64.

Stebbins, J.F. and Xu, Z. (1997) NMR evidence for excess non-bridging oxygen in an aluminosilicate glass. *Nature* **390**, 60-62.

Taylor, S.R. and McLennan, S.M. (1995) The geochemical evolution of the continental crust. *Reviews of Geophysics* **33**, 241-265.

Wedepohl, K.H. (1995) The composition of the continental crust. *Geochimica Et Cosmochimica Acta* **59**, 1217-1232.

White, W.M. and Klein, E.M. (2014) 4.13 - Composition of the Oceanic Crust A2 - Holland, Heinrich D, in: Turekian, K.K. (Ed.), Treatise on Geochemistry (Second Edition). Elsevier, Oxford, pp. 457-496.

Appendix

Appendix A1. Quantum chemical calculations

Quantum chemical calculations were performed with the Gaussian 03 program (Frisch et al., 2004). To check the effect of sodium on the ^{11}B NMR shielding of non-ring ($^{[3]}B$), two series of $^{[3]}BO_3$ model clusters were used: one is $^{[3]}BO_3$[xNa, (3-x)H], in which hydrogen was used to compensate the charge, where x is the number of Na attached to the cluster, and the other is $^{[3]}BO_3$[xNa, (3-x)$^{[3]}B(OH)_2$] in which the effect of hydrogen on $^{[3]}B$ was reduced with a bigger cluster, where x is the number of Na attached to the cluster. Figure A1 illustrates the optimized configurations for all the clusters. Figure A1 A~D show $^{[3]}BO_3$[xNa, (3-x)H] model cluster with varying the number of sodium. Figure A1 E~H show $^{[3]}BO_3$[xNa, (3-x)$^{[3]}B(OH)_2$] model cluster with varying the number of sodium. Cluster geometry optimizations were executed at the B3LYP (Becke, three-parameters, Lee-Yang-Parr) hybrid density functional theory method with a 6-311+G(2d,p) basis for all the clusters (Becke, 1993). Table A1 shows the optimized geometry information of $^{[3]}BO_3$[xNa, (3-x)H] and $^{[3]}BO_3$[xNa, (3-x)$^{[3]}B(OH)_2$] clusters with the number of Na (x) calculated in this study. The NMR shielding of each cluster was calculated at the B3LYP/6-311+G(2d,p) level. It should be noted that the multiplicity used in this study was 3 for $^{[3]}BO_3$[xNa, (3-x)H] model cluster.

Fig. A2 shows the ^{11}B isotropic chemical shielding of $^{[3]}BO_3$[xNa, (3-x)H] with varying the number of Na attached to the cluster. The ^{11}B isotropic chemical shielding increases with the presence of Na and then decreases with increasing the number of Na. An increase in the ^{11}B isotropic chemical shielding with x=1 seems to be due to the hydrogen effect which can affect the electronic structure of $^{[3]}B$ within the distance between H and $^{[3]}B$ in this model cluster. To eliminate the hydrogen effect, ^{11}B isotropic chemical shielding of a bigger clusters ($^{[3]}BO_3$[xNa, (3-x)$^{[3]}B(OH)_2$]) was calculated. Fig. A2 shows the ^{11}B isotropic chemical shielding of $^{[3]}BO_3$[xNa, (3-x)$^{[3]}B(OH)_2$] with varying x. As the number of Na increases, ^{11}B isotropic chemical shielding decreases, indicating that the ^{11}B NMR chemical shift of non-ring ($^{[3]}B$) increases with increasing sodium content. It should be noted that the tendency of a decrease is valid rather than the absolute value of the change in ^{11}B isotropic chemical shielding. These results propose the new interpretation of ^{11}B MAS NMR, thus, the changes of ^{11}B MAS and 3QMAS NMR spectra for Na_2O-B_2O_3 glasses with varying

composition are not due to an increase or decrease of non-ring ($^{[3]}$B) peak, which is based from the previous peak assignment of B_2O_3-SiO_2 glasses, but due to the change in ^{11}B NMR chemical shift with varying sodium, which was suggested in (Lee and Lee, 2016).

Table A1. Optimized geometry information of $^{[3]}BO_3$[xNa, (3-x)H] and $^{[3]}BO_3$[xNa, (3-x)$^{[3]}B(OH)_2$] clusters using B3LYP/6-311+(2d,p) as basis function. X is the number of Na attached to the clusters.

$^{[3]}BO_3$[xNa, (3-x)H]			
		B-O (Å)	^{11}B NMR chemical shielding
X	0	1.369	81.31
	1	1.384	82.76
	2	1.395	80.62
	3	1.398	76.39
$^{[3]}BO_3$[xNa, (3-x)$^{[3]}B(OH)_2$]			
		B-O (Å)	^{11}B NMR chemical shielding
X	0	1.365	73.80
	1	1.405	68.22
	2	1.392	64.25
	3	1.398	60.46

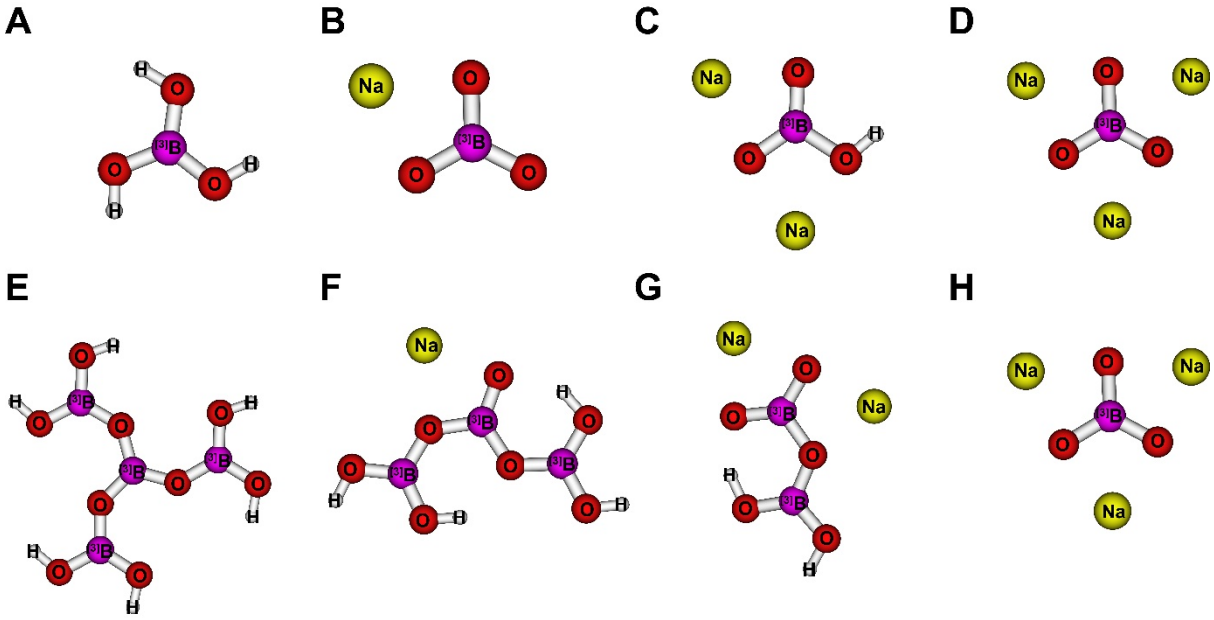

Figure A1. Optimized geometries of $^{[3]}BO_3$[xNa, (3-x)H] and $^{[3]}BO_3$[xNa, (3-x)$^{[3]}B(OH)_2$] clusters with the number of Na (x) at the B3LYP/6-311+(2d,p) level of theory. A~D show the optimized geometries of $^{[3]}BO_3$[xNa, (3-x)H] with x=0, 1, 2, 3. F~H show the optimized geometries of $^{[3]}BO_3$[xNa, (3-x)$^{[3]}B(OH)_2$] with x=0, 1, 2, 3. The atoms in order of decreasing size are Na, B, O, and H. Bond lengths and angles are given in Table A1.

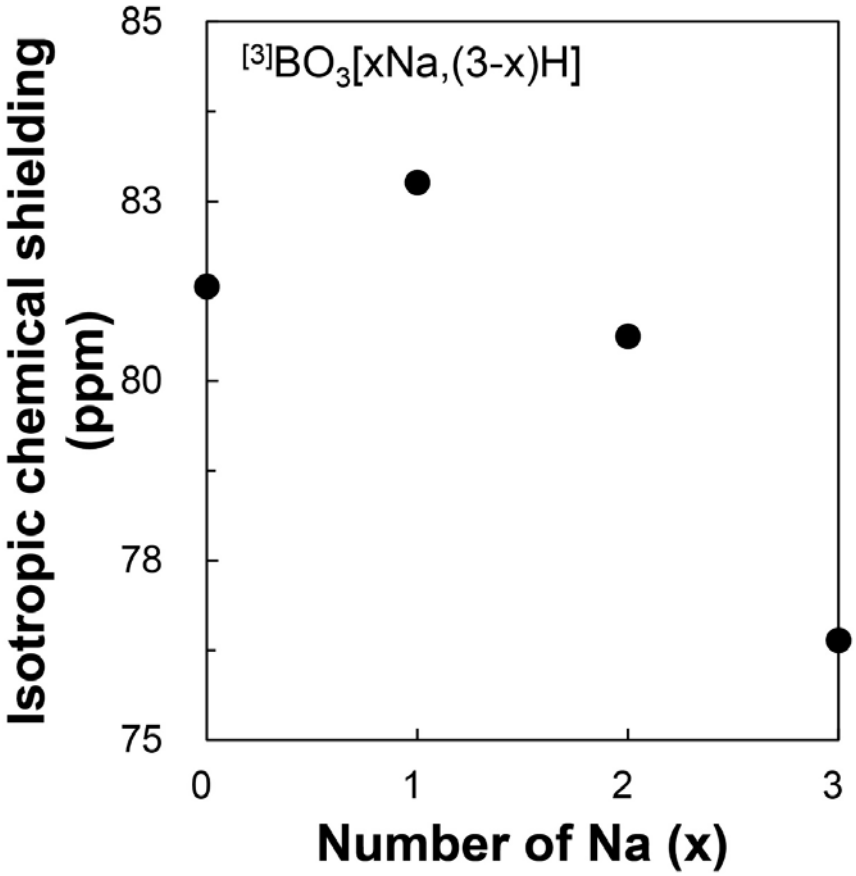

Figure A2. The ^{11}B isotropic chemical shielding of $^{[3]}BO_3$[xNa, (3-x)H] clusters with the number of Na (x).

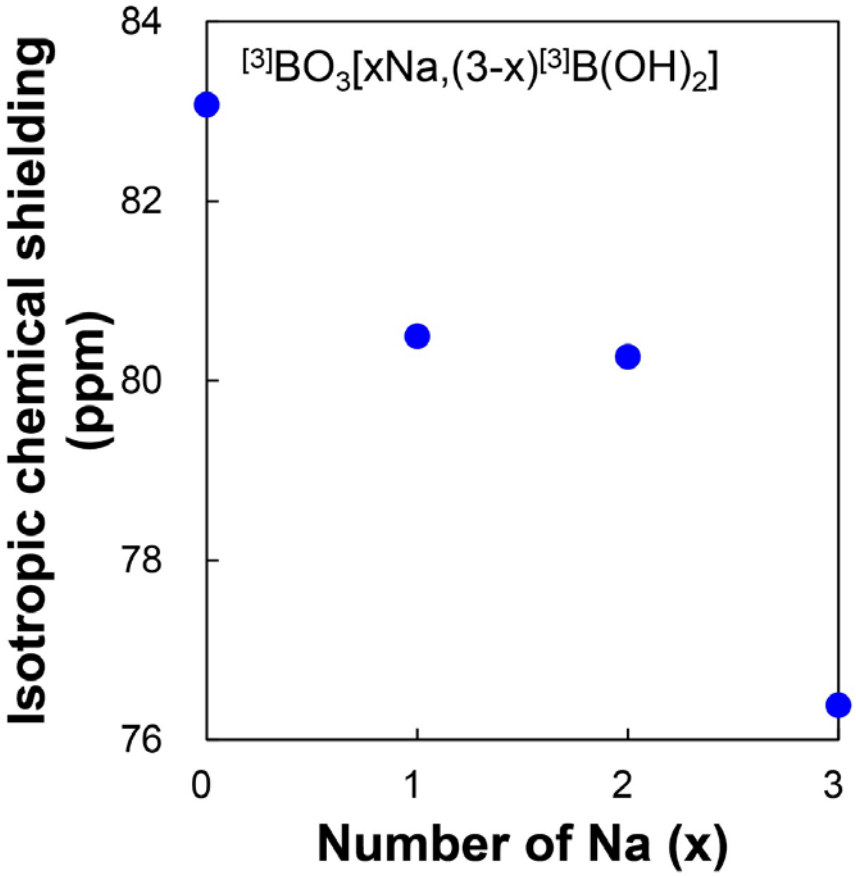

Figure A3. The ^{11}B isotropic chemical shielding of $^{[3]}BO_3[xNa, (3-x)^{[3]}B(OH)_2]$ clusters with the number of Na (x).

Appendix A2. Simulation of ^{11}B MAS NMR spectra for boron-bearing nepheline and albite glasses

The quantification of boron species for boron-bearing nepheline and albite glasses in this study was performed by fitting ^{11}B MAS NMR spectra of each glass using the Dmfit software (Massiot et al., 2002). The fitting function *Q MAS 1/2* that specializes in fitting quadrupolar nucleus like boron was chosen. Because $^{[3]}B$ and $^{[4]}B$ peaks are not fully resolved in ^{11}B MAS NMR spectra at 9.4 T, ^{11}B 2D 3QMAS NMR spectra were also referred to fit the results. The fitting parameters of ^{11}B MAS NMR spectra for $NaAlSiO_4$-$NaBSiO_4$, and $NaAlSi_3O_8$-$NaBSi_3O_8$ glasses are shown in Table A2 and A3, respectively. Figure A4~7 show the simulation results, where thin black, red, and green lines refer total simulations, non-ring ($^{[3]}B$) species, and $^{[4]}B$ species, respectively, of ^{11}B MAS NMR spectra for $NaAlSiO_4$-$NaBSiO_4$ glasses with varying X_{Ma}. Figure A8~11 show the simulation results, where thin black, red, and green lines refer total simulations, non-ring ($^{[3]}B$) species, and $^{[4]}B$ species, respectively, of ^{11}B MAS NMR spectra for $NaAlSi_3O_8$-$NaBSi_3O_8$ glasses with varying X_{Rd}.

Table A2. Fitting parameters and results of ^{11}B MAS NMR spectra for $NaAlSiO_4$-$NaBSiO_4$ glasses. X_{Ma} is the mole fraction of malinkoite component.

Composition		Species	Intensity	Fraction	Em (a.u.)	δ_{iso} (ppm)	C_q (MHz)	η
X_{Ma}	0.25	Non-ring ($^{[3]}B$)	328	0.54±0.07	350	17.75	2.750	0.25
		$^{[4]}B$	285	0.46±0.07	650	2.00	1.100	0.80
	0.50	Non-ring ($^{[3]}B$)	125	0.23±0.07	400	17.50	2.750	0.20
		$^{[4]}B$	425	0.77±0.07	650	2.00	1.100	0.80
	0.75	Non-ring ($^{[3]}B$)	75	0.14±0.07	350	18.00	2.750	0.20
		$^{[4]}B$	475	0.86±0.07	650	2.00	1.100	0.80
	1	Non-ring ($^{[3]}B$)	65	0.11±0.07	350	18.25	2.750	0.20
		$^{[4]}B$	510	0.89±0.07	650	2.00	1.100	0.80

Table A3. Fitting parameters and results of ^{11}B MAS NMR spectra for $NaAlSi_3O_8$-$NaBSi_3O_8$ glasses. X_{Rd} is the mole fraction of reedmergnerite component.

Composition		Species	Intensity	Fraction	Em (a.u.)	δ_{iso} (ppm)	C_q (MHz)	η
X_{Rd}	0.25	Non-ring ($^{[3]}B$)	197	0.29±0.07	330	15.22	2.750	0.25
		$^{[4]}B$	482.18	0.71±0.07	650	0.52	1.100	0.80
	0.50	Non-ring ($^{[3]}B$)	90	0.16±0.07	330	14.84	2.750	0.25
		$^{[4]}B$	480	0.84±0.07	600	0.5	1.125	0.80
	0.75	Non-ring ($^{[3]}B$)	80	0.14±0.07	400	15.18	2.750	0.25
		$^{[4]}B$	500	0.86±0.07	600	0.5	1.125	0.70
	1	Non-ring ($^{[3]}B$)	51.09	0.09±0.07	400	16.11	2.750	0.25
		$^{[4]}B$	535	0.91±0.07	600	0.4	1.125	0.70

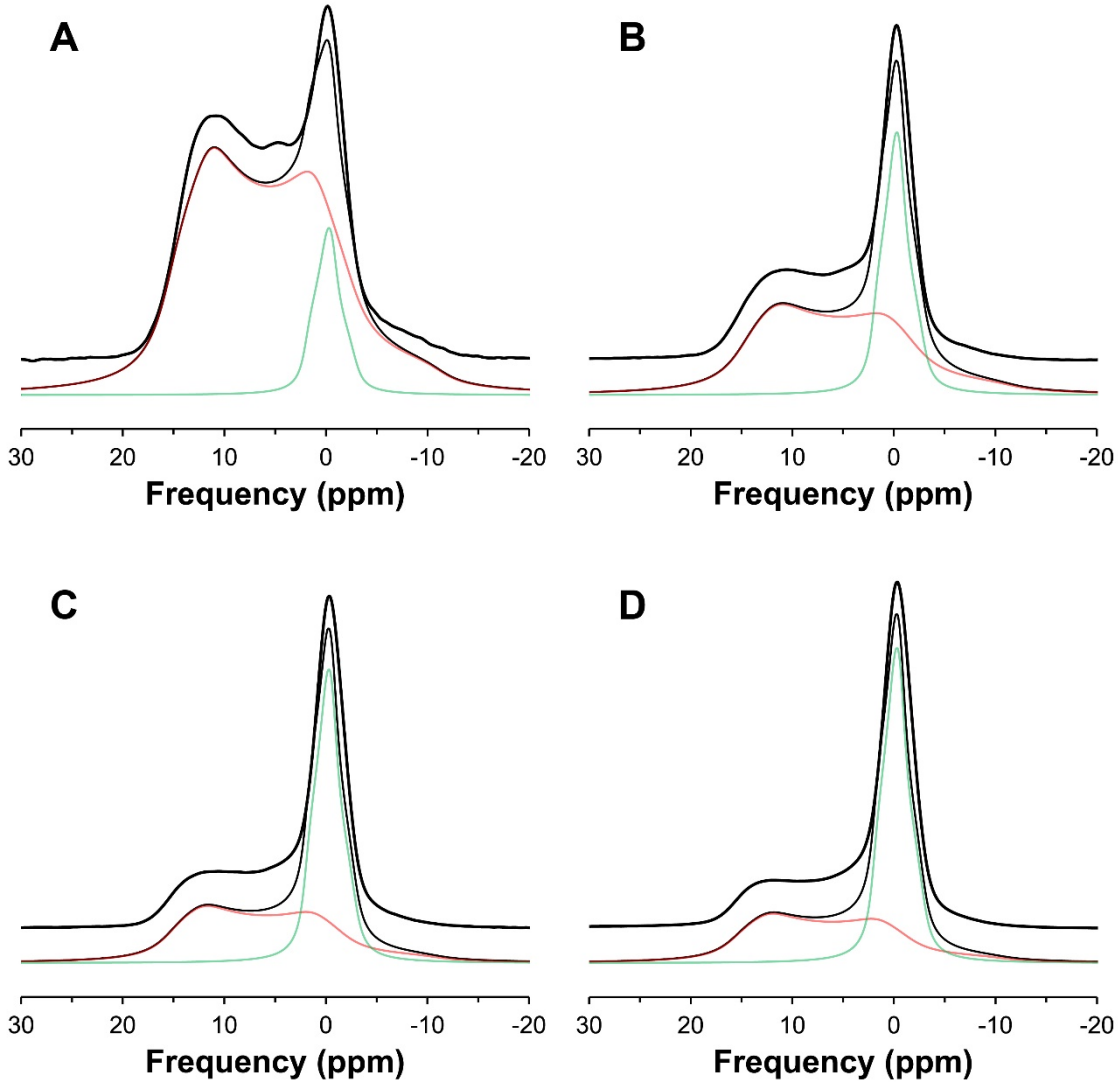

Figure A4. The simulation results, where thin black, red, and green lines refer total simulations, non-ring ($^{[3]}$B) species, and $^{[4]}$B species, respectively, and ^{11}B MAS NMR spectrum (bold black line) for $NaAlSiO_4$-$NaBSiO_4$ glasses with X_{Ma}=0.25 (A), 0.50 (B), 0.75 (C), and 1 (D).

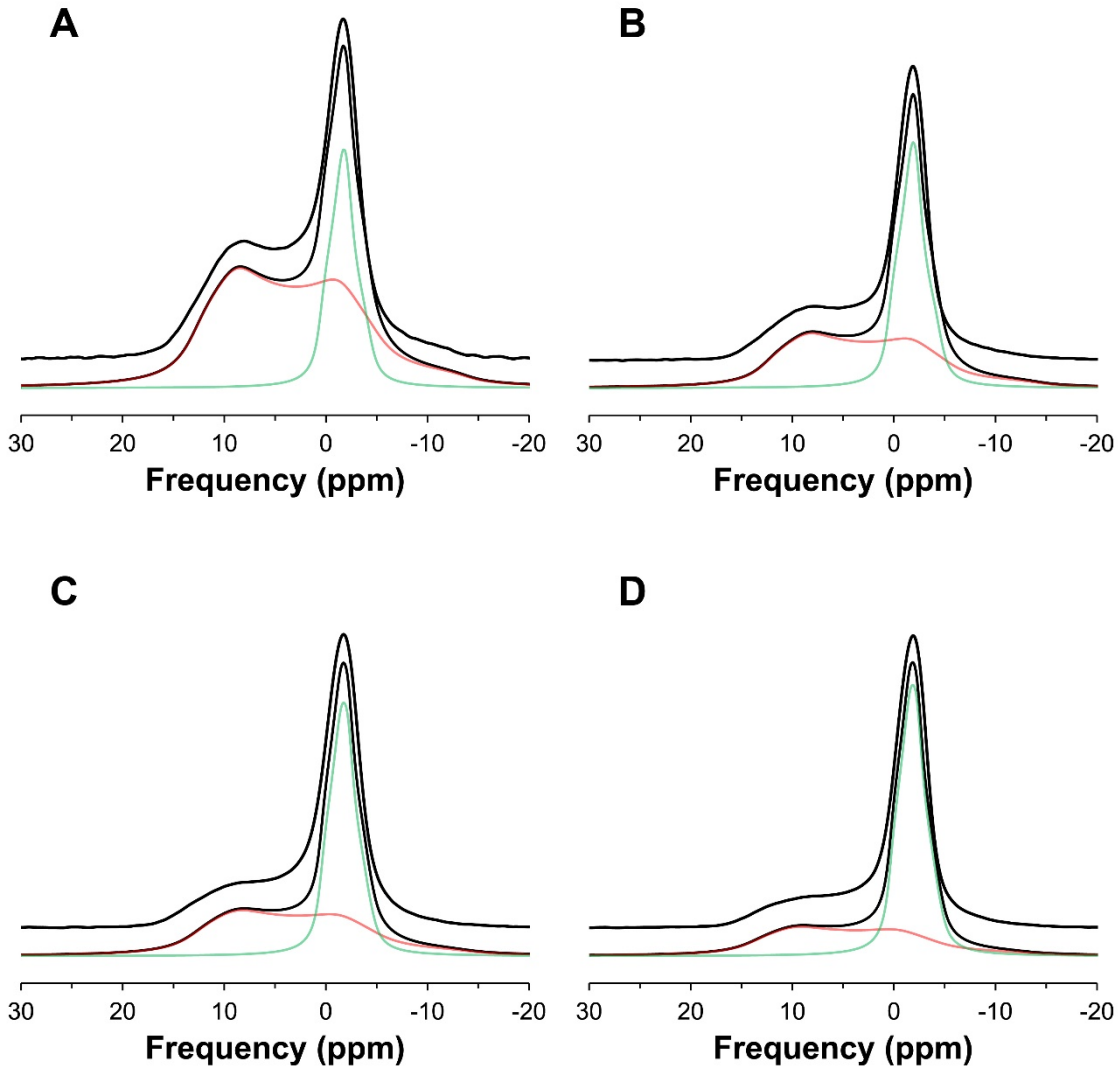

Figure A5. The simulation results, where thin black, blue, red, and green lines refer total simulations, ring ($^{[3]}$B) species, non-ring ($^{[3]}$B) species, and $^{[4]}$B species, respectively, and ^{11}B MAS NMR spectrum (bold black line) for $NaAlSi_3O_8$-$NaBSi_3O_8$ glasses with X_{Rd}=0.25 (A), 0.50 (B), 0.75 (C), and 1 (D).

Appendix A3. FWHM results of ^{27}Al MAS NMR spectra and MAS and isotropic dimension from ^{27}Al 3QMAS NMR spectra for $NaAlSiO_4$-$NaBSiO_4$ glasses with varying X_{Ma}.

It is shown in Park and Lee (2014) how to derive C_q from ^{27}Al 3QMAS NMR spectra in detail. The quadrupolar coupling constant (C_q) was calculated from MAS and isotropic dimension from ^{27}Al 3QMAS NMR spectra for $NaAlSiO_4$-$NaBSiO_4$ glasses with varying X_{Ma}. Figure A12 shows the FWHM results from ^{27}Al MAS NMR spectra for $NaAlSiO_4$-$NaBSiO_4$ glasses with varying X_{Ma}. Figure A13 shows the FWHM results from MAS dimension of ^{27}Al 3QMAS NMR spectra for the same glasses. The difference between Figure A12 and A13 might be derived of uncertainties of phasing and overlap of $^{[4]}$Al and $^{[5]}$Al peaks for the glasses with X_{Ma}=0.75. Figure A14 shows the FWHM results from isotropic dimension of ^{27}Al 3QMAS NMR spectra for the same glasses. Table A4 shows the FWHM and NMR parameters from ^{27}Al MAS and 3QMAS NMR spectra for $NaAlSiO_4$-$NaBSiO_4$ glasses with varying $X_{Ma.}$

Table A4. The FWHM and NMR parameters from ^{27}Al MAS and 3QMAS NMR spectra for $NaAlSiO_4$-$NaBSiO_4$ glasses with varying $X_{Ma.}$ η was assumed to be 0.5.

Composition		MAS dimension from ^{11}B MAS NMR spectra (ppm)	Isotropic dimension from ^{11}B 3QMAS NMR spectra (ppm)	MAS dimension from ^{11}B 3QMAS NMR spectra (ppm)
X_{Ma}	0	26.88±0.3	12.91±0.3	23.88±0.3
	0.25	21.05±0.3	9.00±0.3	19.82±0.3
	0.50	20.64±0.3	8.58±0.3	19.82±0.3
	0.75	20.61±0.3	8.09±0.3	20.40±0.3

Composition		Center of gravity (ppm)		δ_{iso}^{2Q} (ppm)	δ_{iso}^{CS} (ppm)	P_q (MHz)	C_q (MHz)
		MAS dimension	Isotropic dimension				
X_{Ma}	0	49.19±0.3	-40.37±0.3	-15.38	64.57	5.28	5.07
	0.25	51.10±0.3	-38.33±0.3	-11.83	62.93	4.63	4.45
	0.50	50.16±0.3	-37.56±0.3	-11.54	61.70	4.57	4.39
	0.75	52.38±0.3	-39.54±0.3	-12.42	64.80	4.74	4.56

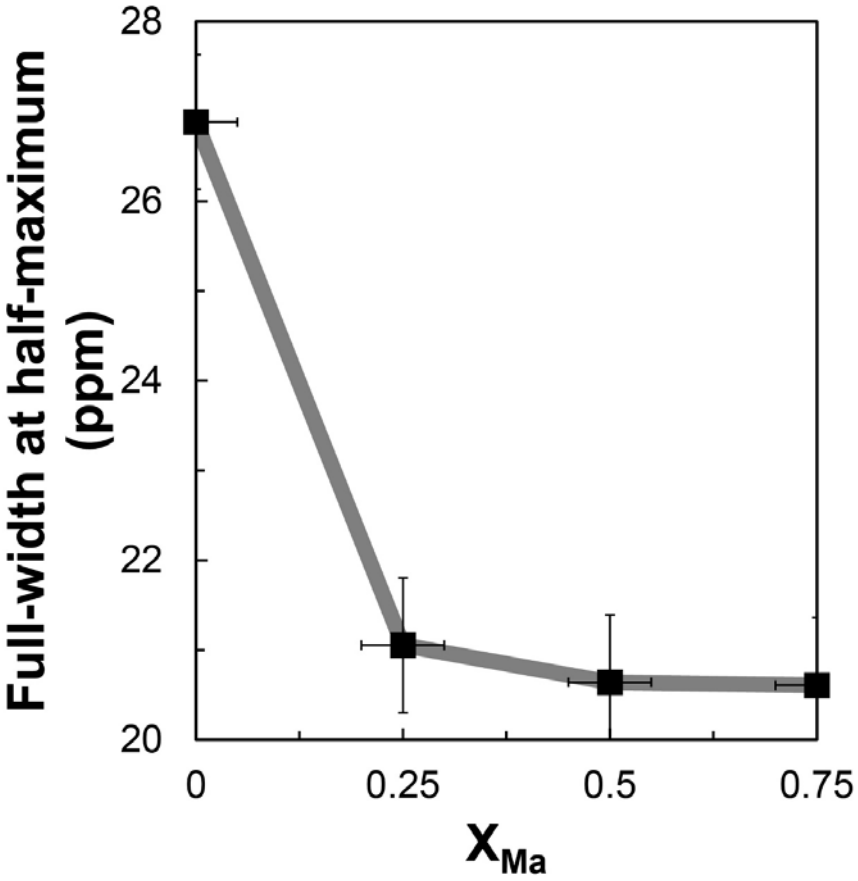

Figure A6. The FWHM results with varying X_{Ma} from ^{27}Al MAS NMR spectra for $NaAlSiO_4$-$NaBSiO_4$ glasses.

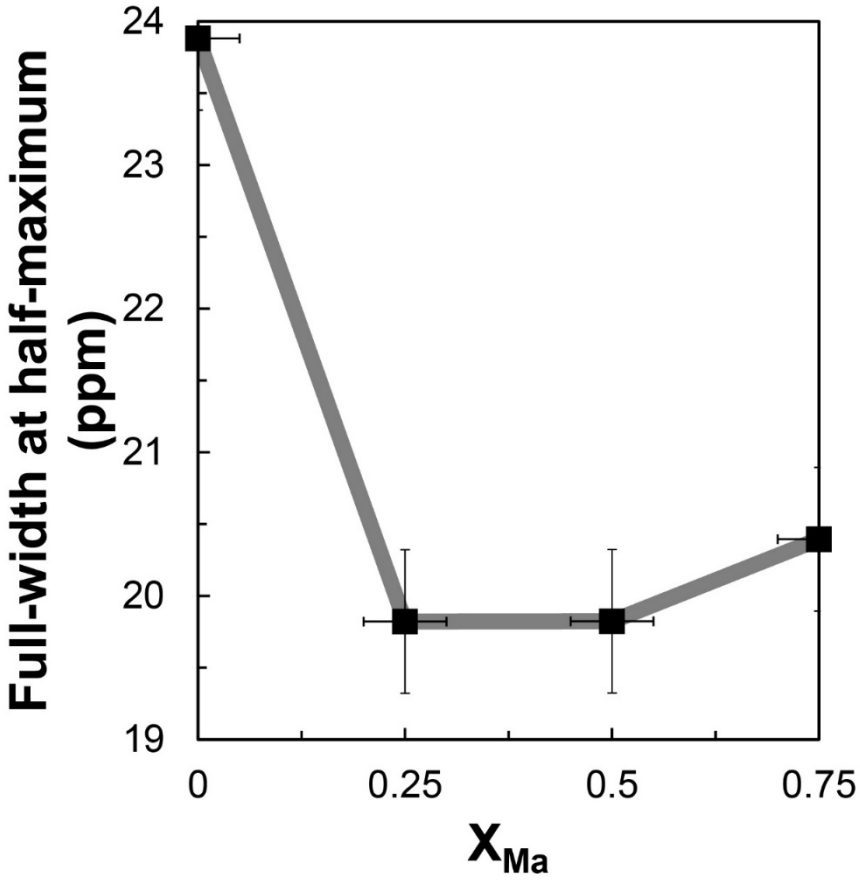

Figure A7. The FWHM results with varying X_{Ma} from MAS dimension of ^{27}Al 3QMAS NMR spectra for $NaAlSiO_4$-$NaBSiO_4$ glasses.

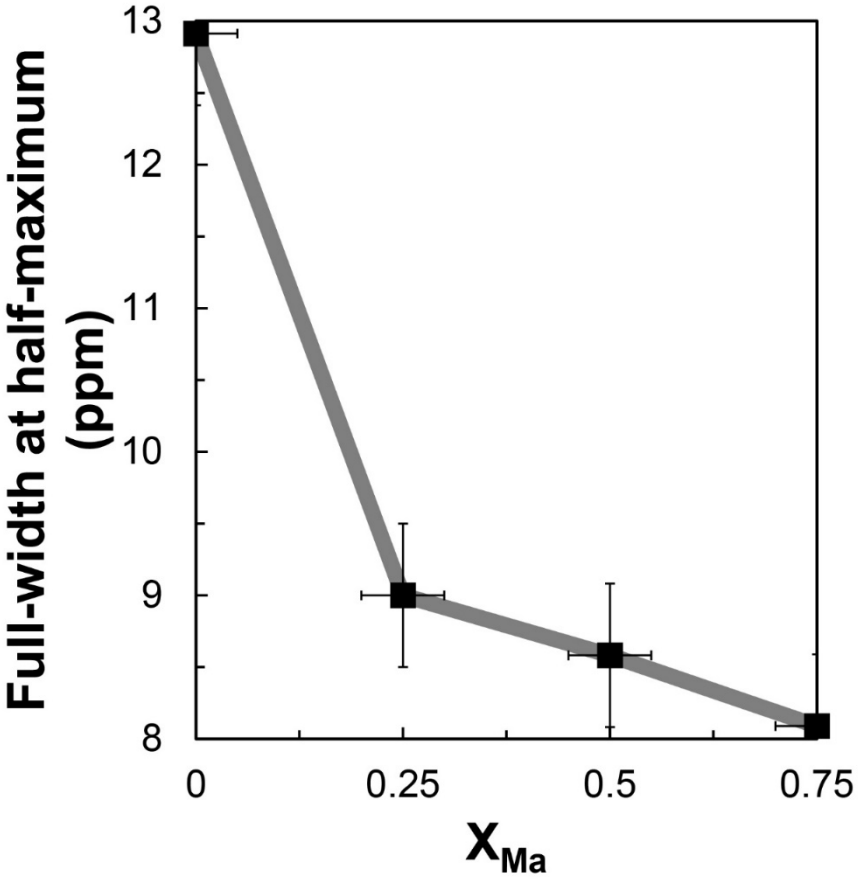

Figure A8. The FWHM results with varying X_{Ma} from isotropic dimension of ^{27}Al 3QMAS NMR spectra for $NaAlSiO_4$-$NaBSiO_4$ glasses.

국문 초록

지구상에서 미량 원소로 존재하는 B(boron)의 조성 및 압력에 따른 분포 및 원자 환경과 이것이 맨틀 용융체에 미치는 영향에 대한 원자 단위의 정보는 지구화학 분야에서 근본적인 문제인 깊이, 온도, 조성에 따른 붕소의 분포 및 원자 구조에 대한 단서를 제공한다. 뿐만 아니라 핵폐기물을 유리를 만드는데 B_2O_3가 이용되기 때문에 환경지구화학에서도 B에 의한 유리의 안정도는 매우 중요하게 여겨진다. B_2O_3는 약 5 wt%의 존재로도 화강암질 마그마의 점성도를 수 천 배 정도 낮추므로, 마그마의 이동을 용이하게 한다. 또한 B의 함량이 많을수록 비정질 규산염에서 용해 속도가 급증하고, 이는 마그마가 바다에 분출했을 때 B를 많이 함유할수록 수용액과 더 반응한다는 것을 의미한다. B가 이동 물성에 큰 영향을 미치지만 이동 물성의 변화를 설명하는 원자 구조에 대한 정보는 난제로 남아 있다. 그 이유는 원자 구조에 대한 정보를 제공하는 방법론이 부족하고 네트워크를 형성하지 않는(non-framework cation) 이온이 포함된 비정질 규산염의 B 원자 환경이 규명되지 않았기 때문이다. 따라서 본 연구에서는 양자 화학 계산을 통해 B의 NMR 화학 차폐값이 Na의 함량이 많아 질수록 증가한다는 것을 통해 이전 연구들과는 달리 Na가 증가하면 ring ($^{[3]}$B)이 $^{[4]}$B로 전환되고, non-ring ($^{[3]}$B) 구조가 감소하지 않고 일정하다고 해석하였다. 비정질 $NaAlSiO_4$-$NaBSiO_4$ 과 $NaAlSi_3O_8$-$NaBSi_3O_8$ 유사이원계에서 높은 Na/B 비율로 인해 ring ($^{[3]}$B) 구조가 존재하지 않는다고 가정하였고, ^{11}B NMR 결과를 통해 non-ring ($^{[3]}$B)가 감소하여 $^{[4]}$B가 생성된다는 것을 밝혔고 B의 원자 환경 변화를 정량 분석 하였다. B의 원자 환경 변화로 인해 용해도가 바뀐다는 이전에 제시된 기작과는 달리 B의 원자 환경 변화가 용해도 변화를 설명할 수 없었고, ^{17}O NMR 실험을 통해 B를 함유한 다성분계 규산염 용융체의 산소 원자 환경 분석을 하여, Na-O-Si, B-O-B와 B-O-$^{[4]}$Si가 B의 함량에 따라 증가하는 것을 밝혔다. NBO의 증가는 규산염 용융체의 낮은 중합도를 설명하므로, Na-O-$^{[4]}$Si로 인해 B를 함유한 화강암질 마그마의 점성도 감소를 설명할 수 있을 것으로 생각된다. B의 용해도에 영향을 줄 것으로 생각되었던 Na-O-B가 매우 적은 것이 관찰되었고, 따라서 연결 산소 중 상대적으로 약한 결합인 B-O-B와 B-O-$^{[4]}$Si 결합이 끊어지면서 B의 용해가 일어날 것으로 생각된다.